J. Fluid Mech. (1982), *vol.* 115, *pp.* 59-89
Printed in Great Britain

The self-excited axisymmetric jet

By M. A. Z. HASAN AND A. K. M. F. HUSSAIN
Department of Mechanical Engineering, University of Houston, Texas 77004

(Received 25 January 1980 and in revised form 2 February 1981)

The characteristics of a self-excited axisymmetric air jet driven by a whistler (i.e. pipe-collar) nozzle have been explored experimentally for various choices of the controlling parameters: namely, pipe length, jet diameter, collar length, step height, and jet speed. By appropriate choices of these parameters as well as the stage and mode (half- and full-wave), the self-sustained excitation has been induced at specific values of the excitation amplitude and the Reynolds number R_D. The jet characteristics up to $R_D \simeq 3{\cdot}1 \times 10^5$ and $x/D \simeq 60$ have been documented for both laminar and turbulent flows at the pipe exit. Comparison with corresponding unexcited-jet data reveals that self-excitation produces a large increase in the fluctuation intensity in the near field of the jet, while it increases the jet spread and decay rate for the entire x-range of measurement. The dependence of the jet structure on the initial condition is stronger when self-excited than when unexcited. The first stage of excitation always produces the highest turbulence augmentation and the spectral evolution is significantly modified by self-excitation up to $x/D \simeq 6$. The excitation produces a significant increase in the broad-band turbulence level over that of the unexcited jet. The broad-band amplification is maximized at $x/D \simeq 4$ and is the highest at the largest R_D studied.

These data suggest interesting possibilities for the self-excited jet in the augmentation or control of entrainment, mixing and aerodynamic noise production.

1. Introduction

Although the role, and even existence, of large-scale coherent structures in turbulent shear flows have not been universally accepted (Chandrsuda *et al.* 1978; Batt 1978; Pui & Gartshore 1979; Clark 1979), these structures have been the focus of tremendous interest among researchers in recent years (Brown & Roshko 1974; Winant & Browand 1974; Browand & Laufer 1975; Davies & Yule 1975; Acton 1980; Moore 1977; Ffowcs Williams & Kempton 1978). There are persistent suggestions from many of these studies that large-scale coherent structures and their interactions play key roles in the transport of heat, mass and momentum, and in the generation of aerodynamic noise. Serious efforts are therefore underway to obtain the detailed characteristics of these structures, with the hope that knowledge of these will lead to a better understanding of turbulent flows as well as to the development of a viable theory of shear-flow turbulence. (For a review of the related questions see Hussain (1981), which also summarizes a few of our results on coherent structures.)

There have been two alternative approaches to the study of these structures. One approach has been to study the naturally occurring ones (Bruun 1977; Yule 1978). However, this approach has a number of constraints, primarily because of the large

dispersion in the shape, size, orientation, strength and convection velocity of these structures. An alternative approach is to induce these structures artificially and educe their details through measurements phase-locked to that excitation which can organize the large-scale structures (Zaman & Hussain 1980; Hussain & Zaman 1980). In most investigations of coherent structures, as well as in studies of shear-layer instability, controlled excitation has been induced with the help of loudspeakers (Freymuth 1966; Miksad 1972; Crow & Champagne 1971; Pfizenmaier 1973), while, in others, periodic-ribbon excitation (Schubauer & Skramstad 1947; Hussain & Reynolds 1970; Khalifa & Hussain 1979), spark generation (Zilberman, Wygnanski & Kaplan 1977; Sokolov *et al.* 1980) or fluid injection (Cantwell, Coles & Dimotakis 1978; Petersen, Kaplan & Laufer 1974; Kibens 1980) have been employed.

Large-scale coherent structure in the circular jet has been the subject of continuing investigation in our laboratory (Hussain & Thompson 1980; Zaman 1978; Clark 1979; Sokolov *et al.* 1980; Zaman & Hussain 1980; Hussain & Zaman 1980; Tso, Kovasznay & Hussain 1980). In the course of our studies of controlled excitation of the circular jet, we came to realize the advantages of inducing controlled perturbation through self-sustained excitation with the whistler nozzle. The attractiveness of the whistler nozzle is its simple geometry and requirement of no external power.

The whistler-nozzle excitation of a jet

The whistler nozzle is a passive device consisting of a constant-diameter tail-pipe, attached to the downstream end of a jet nozzle, and a constant-diameter collar which can slide over the pipe (figure 1*b*). Depending on the step height h (i.e. the difference between the inside radii of the pipe nozzle and the collar), the jet speed U_e and the pipe length L_p, as the collar is gradually pulled out (i.e. moved downstream), the jet produces a loud pure-tone sound; this is the first stage. With increasing collar length L_c (i.e. the streamwise projection of the collar beyond the pipe exit), the frequency of the tone decreases monotonically and the sound strength increases, reaches a peak and then decreases until it disappears. With further increase of L_c, the sound quite abruptly reappears at a slightly lower frequency; this is the second stage (Hasan 1978). The sound is the result of resonance of the pipe nozzle as an open–open organ pipe in either the full-wave mode or the half-wave mode. The process at work is too involved to be reviewed here; the explanation and documentation of the phenomenon will be the subject of another paper. Note that 'mode' refers to half-wave or full-wave organ-pipe resonance of the pipe nozzle while 'stage', as explained above, denotes the same as in any edge-tone system.

Hill & Greene (1977) appear to be the first to have discovered the whistler-nozzle operation. They studied this for limited ranges of the parameters, but were unable to find any correlation between the parameters and concluded that no general correlation behaviour could be determined. From our more extensive data, we were able to show (Hasan & Hussain 1979) that the controlling parameters can be related as follows:

$$\frac{f}{a_0 n}\left(L_p + 1{\cdot}65\frac{L_c}{j} + 0{\cdot}7D\right) = 1, \tag{1}$$

where a_0 is the acoustic speed, n ($=\frac{1}{2}$ or 1) denotes the mode and j ($=1, 2, 3, \ldots$) the stage. The second and third terms on the left-hand side of (1) are the corrections to the pipe length: one due to the stage of excitation and the collar length L_c (which also

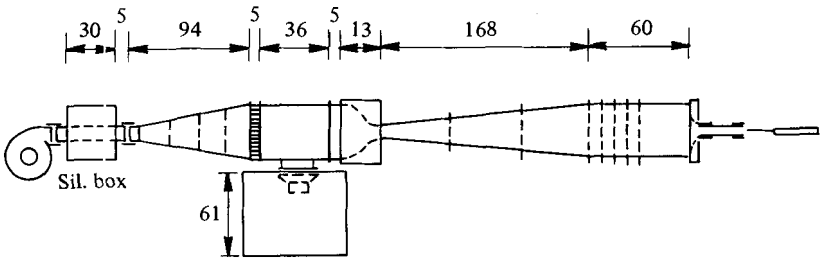

(*a*)

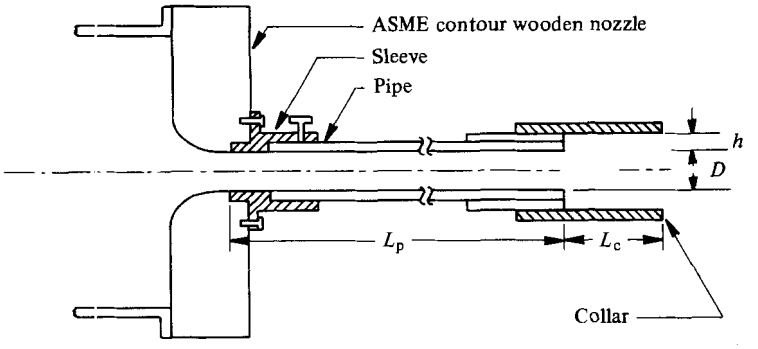

(*b*)

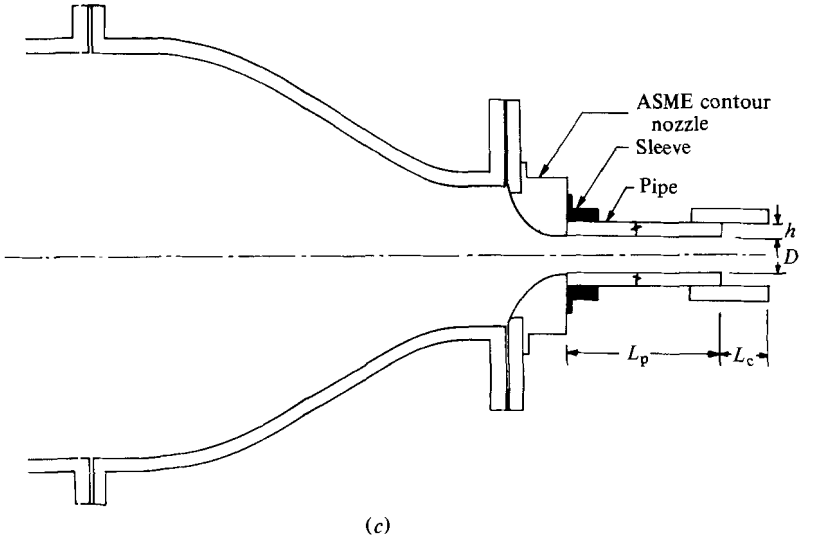

(*c*)

FIGURE 1. (*a*) Schematic of the 2·54 cm diameter jet facility. (*b*) Details of the whistler nozzle. (*c*) Schematic of the whistler-nozzle arrangement for the 7·62 cm diameter jet.

includes the effects of h, as larger h requires larger L_c), and the other due to the diameter D. The two constants (1·65 and 0·70) were obtained from a least-squares fit of data for 32 different cases. The standard deviation of the left-hand side of (1) was within 0·003 for all data. Hill & Greene also presented some data on the jet response; however, the exit excitation amplitude u'_e/U_e (u' is the r.m.s. of the longitudinal-

fluctuation velocity u; u'_e is the exit centre-line value of u') was not held constant nor was the initial condition documented. The jet response to a whistler-nozzle excitation can be characterized meaningfully only if the excitation is controlled. The primary objective of this study was to document the jet response to self-excitation (at controlled u'_e/U_e) and the sensitivity of this response to the initial condition and R_D. It was also felt that the results would find use in the control of mixing and aerodynamic noise in a jet.

2. Apparatus and procedure

The experiments have been carried out in two separate air-jet flow facilities located in a large laboratory with controlled temperature and humidity. The ambient draught and turbulence are not likely to be major factors in the jet data (Kotsovinos 1976; Bradshaw 1977). Most of the data presented have been obtained through an on-line computer (HP 2100S) under remote control so that the data are also free from operator-induced disturbances. The majority of the data were taken in a 2·54 cm diameter axisymmetric air jet. The jet configuration, consisting of two settling chambers in tandem (figure 1(*a*)), was designed in connection with the controlled external excitation of the circular jet (see Zaman & Hussain 1980). The two settling chambers (each of 25 cm diameter) and the diffusers are fitted with a number of 12 mesh/cm screens spaced at appropriate intervals. The second settling chamber assures the axisymmetry of the flow upstream of the whistler nozzle. The dimensions of the facility in figure 1 (*a*) are in cm. Figure 1 (*b*) shows the details of the whistler nozzle, which is attached to the end of the settling chamber following an ASME nozzle at the centre of an end plate. For $D = 2{\cdot}54$ cm, data were taken with six different pipe lengths L_p for two values of the step height, $h = 0{\cdot}3175$ cm and 0·635 cm. For $D = 2{\cdot}54$ cm, the whistler-jet operation could not be induced for L_p larger than 91·44 cm (i.e. $L_p/D = 36$). Additional, less-extensive data were taken with a 7·62 cm diameter pipe nozzle in a large (27 cm) diameter jet-flow facility described by Husain & Hussain (1979). The transition from the 27 cm nozzle to the 7·62 cm diameter whistler nozzle was obtained through an ASME nozzle (figure 1(*c*)). Data in the 7·62 cm diameter pipe nozzle were obtained for two different values of L_p (i.e. 30·48 and 60·96 cm) and the step height $h = 0{\cdot}635$ cm.

The two jet facilities are driven by full-wave rectifier-controlled d.c. motors which can hold the jet speeds constant over long runs. The data have been obtained with a tungsten hot wire of diameter 4 μm, operated by a linearized constant-temperature anemometer (DISA) at an overheat ratio of 0·4. The frequency spectra were obtained with a real-time spectrum analyser (Spectrascope model SD335 with 500 lines in selectable frequency ranges up to 50 kHz). The uncertainty of the frequency data is $\pm 0{\cdot}5\,\%$ of the full scale. The spectrum $S_u(f)$ plotted is defined such that $\int_0^\infty S_u^2(f)\,df = \overline{u^2}$. Data were obtained with a precision backlash-free traversing mechanism operated through stepping motors which were driven on-line by the laboratory computer.

Note that the origin of the co-ordinates is located at the centre of the pipe-nozzle exit for both excited and unexcited cases; x increases downstream and y increases radially.

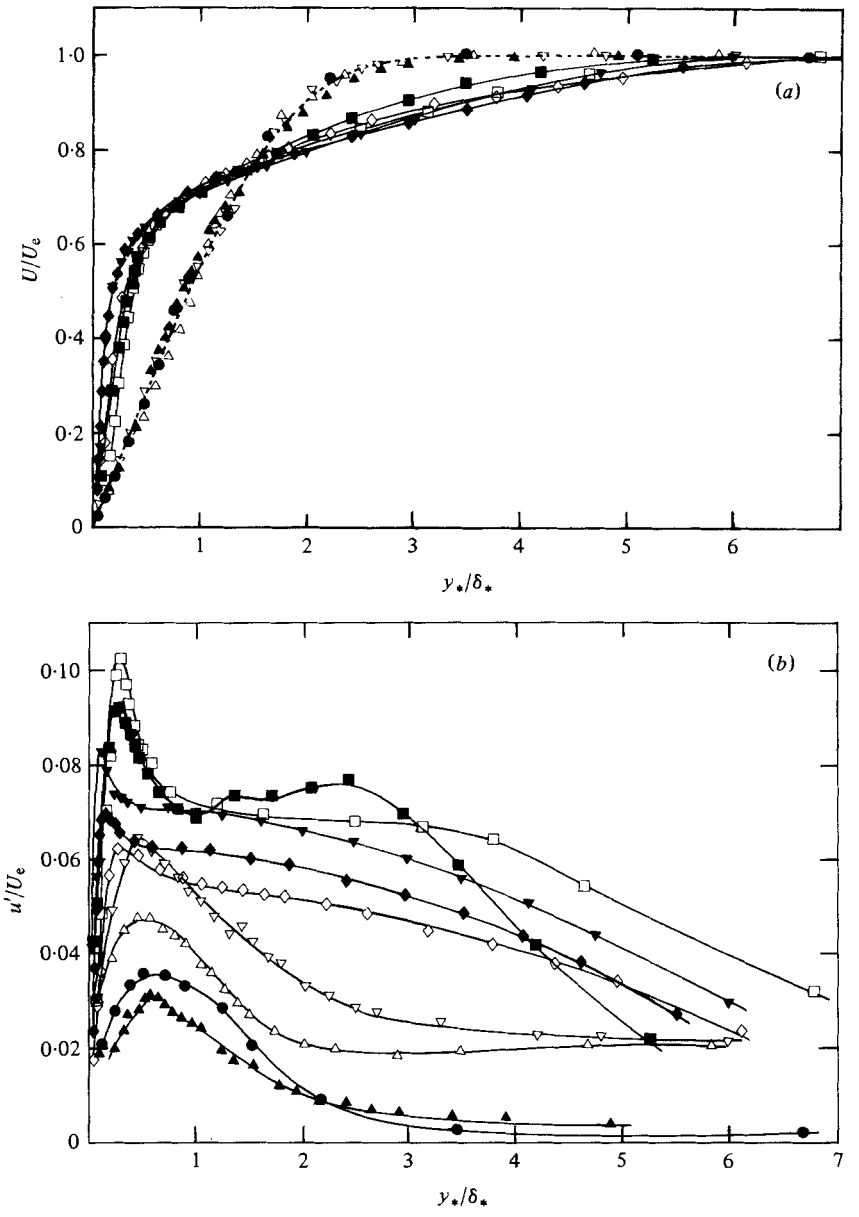

FIGURE 2. (*a*) Boundary-layer mean velocity profiles at the pipe exit for $D = 2{\cdot}54$, $U_e = 36$ m s^{-1}. Nozzle length L_p(cm) and stage of excitation are: ●, 7·62 (0); ▲, 15·24 (0); △, 15·24 (I); ▽, 15·24 (II); ■, 30·48 (0); □, 30·48 cm (I); ◆, 60·96 (0); ▼, 91·44 (0); ◇, 15·24 (tripped, 0) ---, Blasius profile. Excitation cases are for $u_e'/U_e = 3\,\%$. (*b*) Longitudinal-fluctuation-intensity profiles of the pipe-exit boundary layer. Symbols as in (*a*).

3. Results and discussion

Initial condition

Unless otherwise stated, data reported in this paper are for the $D = 2{\cdot}54$ cm pipe at $U_e = 36$ m s^{-1}, corresponding to R_D $(= U_e D/\nu) = 6{\cdot}2 \times 10^4$. In order to understand how the jet is modified by self-excitation, it is important to document the initial

U_e (m s^{-1})	L_p (cm)	D (cm)	Stage	δ_* (cm)	θ (cm)	H
36	7·62	2·54	0	0·0394	0·0145	2·728
36	15·24	2·54	0	0·0559	0·0218	2·56
36	15·24	2·54	I	0·Q437	0·0165	2·64
36	15·24	2·54	II	0·0424	0·017	2·512
36	30·48	2·54	0	0·0719	0·0422	1·703
36	30·48	2·54	I	0·0592	0·0391	1·511
36	60·96	2·54	0	0·1397	0·1014	1·378
36	91·44	2·54	0	0·2037	0·140	1·454
36	15·24 (tripped)	2·54	0	0·0653	0·045	1·457
36	30·48	7·62	0	0·0615	0·0412	1·492
60	30·48	7·62	0	0·0721	0·0506	1·43
60	60·96	7·62	0	0·1494	0·1064	1·403

TABLE 1. Initial-condition parameters

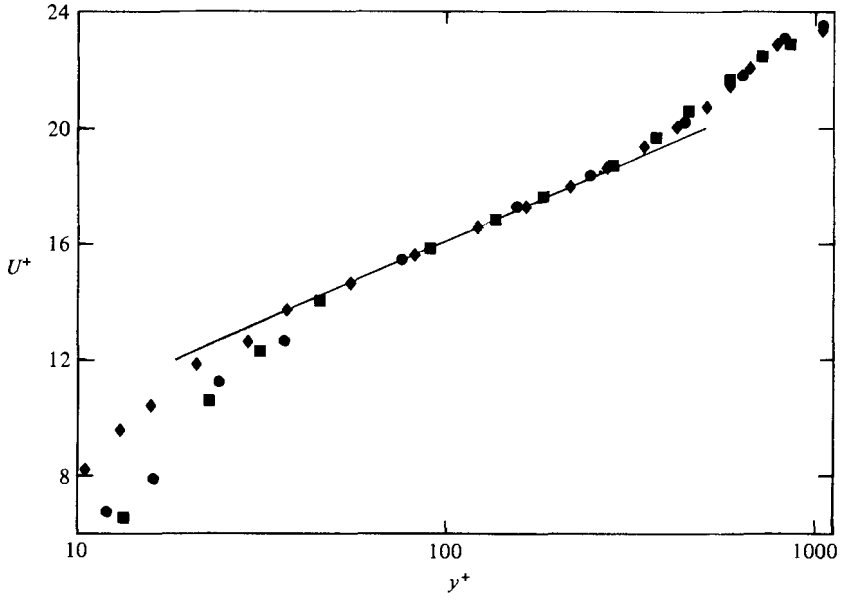

FIGURE 3. Initial mean-velocity distribution at pipe exit in universal co-ordinates (U^+, y^+). L_p (cm), D (cm) and U_e (m s^{-1}) are: ◆, 60·96, 2·54, 36·0; ■, 30·48, 7·62, 60·0; ●, 60·96, 7·62, 60·0. Solid line represents $U^+ = 5{\cdot}6 \log_{10} y^+ + 4{\cdot}9$.

condition for both unexcited and excited cases, because these modifications are most likely to be dependent on the initial condition. Among other measures which characterize the initial condition (Hussain & Zedan 1978), only the mean and r.m.s. longitudinal velocity profiles of the pipe-nozzle exit boundary layer have been used as the identifiers of the initial condition. Figures 2(*a*,*b*) show the mean velocity and longitudinal-fluctuation-intensity profiles at the end of the pipe nozzle (about 1 mm downstream) for all unexcited cases and a few excited cases, the excitation amplitude u_e'/U_e being held at 3 % for all excited cases. The velocity profiles are plotted against $y_* (\equiv \frac{1}{2}D - y)$. When unexcited (i.e. $L_c = 0$), the value of u_e'/U_e – another identifier of the initial condition – was different for different L_p. Values of unexcited u_e'/U_e and

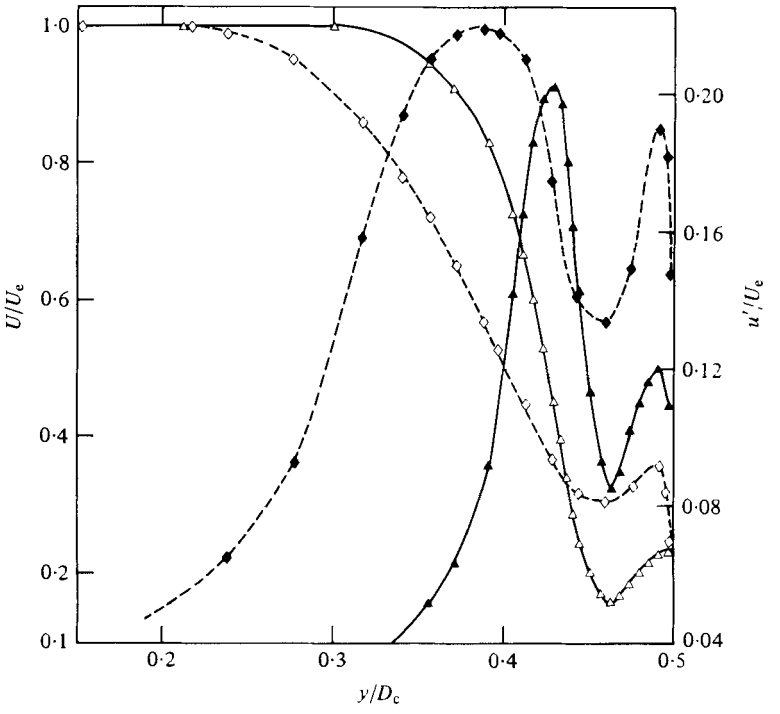

FIGURE 4. Mean-velocity (open) and longitudinal-fluctuation-intensity (solid) profiles at the collar exit. ◆: $L_p = 30{\cdot}48$ cm (I), $D = 2{\cdot}54$ cm, $U_e = 36$ m s^{-1}, $u'_e/U_e = 3\,\%$. ▲: $L_p = 60{\cdot}96$ cm (I), $D = 7{\cdot}62$ cm, $U_e = 60$ m s^{-1}, $u'_e/U_e = 2\,\%$.

the corresponding L_p were as follows: 0·44 % (7·62 cm), 0·66 % (15·24 cm), 0·71 % (30·48 cm), 0·98 % (60·96 cm) and 2·8 % (91·44 cm). The characteristic length scales of the initial boundary layer, namely the displacement thickness $\delta_*[\equiv \int_0^\infty (1 - U/U_e)\,dy]$ and the momentum thickness $\theta[\equiv \int_0^\infty (U/U_e)(1 - U/U_e)\,dy]$, as well as the shape factor $H[\equiv \delta_*/\theta]$ for different L_p, with and without excitation, are presented in table 1. Note that the symbols 0, I and II are used throughout this paper to identify respectively the unexcited stage and the first and second stages of excitation.

The exit boundary layer is laminar for L_p up to 15·24 cm, as suggested by the agreement of the $U(y)$ profiles and shape factors with that of the Blasius profile. For $L_p = 60{\cdot}96$ and 91·44 cm, the exit profiles are turbulent, as suggested by the $u(t)$ signal, the $U(y)$ and $u'(y)$ profiles and the values of the corresponding shape factors (Hinze 1975, p. 633). Note that self-excitation decreases both δ_* and θ (see table 1) and increases the peak value of u'/U_e. The boundary layer for the 7·62 cm diameter pipe was always turbulent within the speed range of interest. Therefore, to compare the effect of self-excitation at a fixed frequency f (hence at fixed L_p) and U_e (i.e. R_D) for two different initial conditions, the exit boundary layer (at $U_e = 36$ m s^{-1}) of the 2·54 cm diameter nozzle of $L_p = 15{\cdot}24$ cm was made turbulent by tripping the flow with a 3 mm long knurled ring inserted at the upstream end of the pipe nozzle. The $U(y)$ and $u'(y)$ profiles for this tripped case are also included in figures 2(*a*, *b*).

Figure 3 shows the mean velocity profiles for the turbulent exit boundary layer in wall co-ordinates ($U^+ \equiv U/U_*$, $y^+ \equiv y_* U_*/\nu$), thus enabling comparison with the

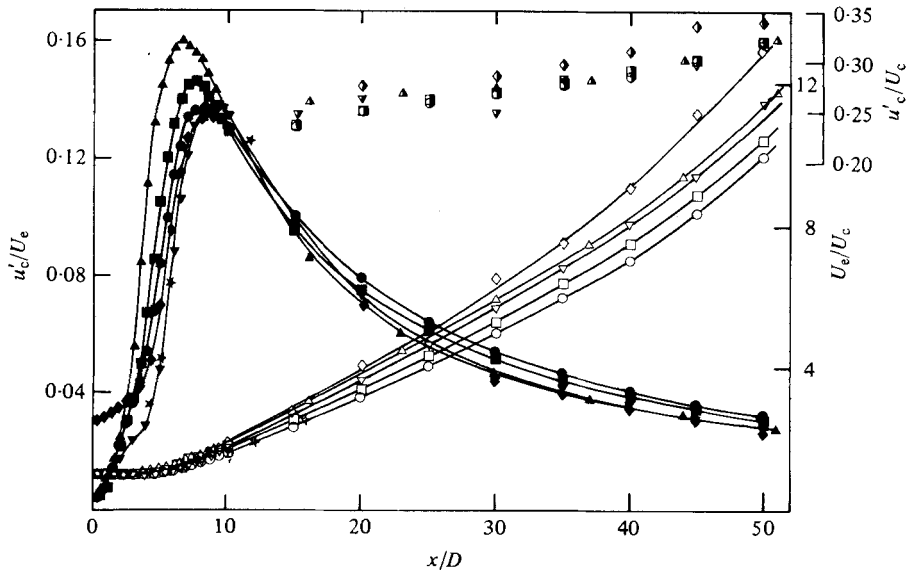

FIGURE 5. Streamwise variations of centre-line values of U_c (open), u_c' (solid) and u_c'/U_c (semi-open), for unexcited cases, D = 2·54 cm and U_e = 36 m s^{-1}. Values of L_p(cm) are: ○, 7·62; □, 15·24; △, 30·48; ▽, 60·96; ◇, 91·44. ☆, Crow & Champagne's (1971) data at R_D = 103000.

equilibrium flat-plate turbulent boundary layer. The friction velocity U_* was determined from the mean-velocity $U(y)$ data by the cross-plot (Clauser-plot) technique. The data in figure 3 are compared with the flat-plate universal formula $U^+ = 5{\cdot}6\log_{10} y^+ + 4{\cdot}9$, and agreements in the logarithmic and wake regions are impressive. The scatter on the low-speed side is to be expected because these data were taken slightly downstream (1 mm) from the pipe exit plane. The wake strength ΔU^+ in the range of 1·7–1·8 for the Reynolds number $U_e\theta_e/\nu$ range 2000–2400 agrees well with that expected for a flat-plate equilibrium boundary layer (Coles 1962). The presence of the prominent wake region, which is typically very weak for bounded fully developed turbulent flows like channel and pipe flows, clearly suggests that, while the boundary layer is fully turbulent, the core flow at the exit had not become the fully developed type of flow. A broad-band spectrum $S_u(f)$ of $u(t)$ in the exit boundary layer, without any peaks, and the centre-line $u(t)$ signal support this claim.

The choice of the pipe exit rather than the collar exit as the initial-condition location has been questioned by a referee and is explained here. First, the boundary layer at the collar exit involves flow reversal which could not be measured with a hot wire. On the other hand, LDA measurement will suffer from poor transverse resolution. The $U(y)$ and $u'(y)$ profiles at the collar exits of both 2·54 and 7·62 cm jets are shown in figure 4 as an example. The peaks in $u'(y)$ near the wall (y/D_c = 0·5) are due to flow reversal, which also produces a distortion of the $U(y)$ profile in each case; D_c is the inside diameter of the collar. Note that values of U and u' are not equal to zero at y/D_c = 0·5 because measurements were made slightly downstream (approx. 1 mm) from the collar exit. Thus, while the pipe exit flow can be accurately characterized, the collar exit flow cannot. Second, the peaks in $u_c'(x)$, plotted as a function of x for different values of $L_c(>0)$ producing *no excitation*, nearly converge if x is measured from the

pipe exit, but vary widely if x is measured from the collar exit. Therefore, while the location at which the initial condition is defined is not very crucial to the physics of the flow, the pipe exit, rather than the collar exit, is the preferred choice for the initial condition.

Furthermore, the difference between the collar wall pressure immediately downstream of the step and the centre-line static pressure was found to be within 2% of the dynamic pressure at the pipe exit centre line. This negligible pressure difference indicates that the momentum fluxes at the collar and pipe exits are essentially equal. (This check was suggested by Dr Bechert.)

Unexcited-jet behaviour

Before considering the jet responses to self-excitation, it is necessary to document the basic (unexcited) states of the jets for various L_p, so that the effects of excitation for each L_p can be identified through comparison. Figure 5 shows streamwise variations of the centre-line mean velocity $U_c(x)$ and r.m.s. longitudinal velocity $u'_c(x)$ for different L_p. The data of Crow & Champagne (1971) (measured for x/D up to 16) are also included for comparison. It is interesting to note that $U_c^{-1}(x)$ does not vary quite linearly with x over the entire x-range studied (as would be expected from consideration of self-preservation (Tennekes & Lumley 1974), even though straight lines can be drawn locally through a few data points.

It is quite likely that U_c^{-1} actually increases linearly with x, but the hot wire gives lower readings at large x (where velocity is low) owing to non-linearity of the linearized curve at low-speed ranges. Perry & Morrison (1971) showed that the exponent n in the hot-wire equation, $E_0^2 = C_1 + C_2 U^n$ (for the voltage E_0 at the velocity U), increases with decreasing U, thus explaining lower U-readings by the hot-wire at lower ranges of calibration. An additional factor that could contribute to this nonlinear variation of U_c^{-1} with x is the possibility that the hot-wire was not located exactly on the local jet axis at each x. Note that the jet centres were first determined from $U(y)$ profiles at $x/D = 10$ and 60 and then data were obtained by traversing the hot wire along the line connecting these two centres. (It should be emphasized that the iterative determination of the exact local jet centre line requires progressively larger times with increasing x, making such identification at all x prohibitively time-consuming.) However, any displacement of the hot wire from the true local centre of the jet is not likely to be critical, since the same radial location (at each x) is used for all data sets. Considering that the principal thrust of this study was to document the jet response to self-excitation (which is significant only in the near field, where either error discussed above will be minimal) the effort that would be necessary for exploring the hot-wire correction and for iterative determination of the centre-line velocity was not considered worthwhile.

In the self-preserving region, one can expect the U_c versus x relation to be $U_c/U_e = A[D/(x+x_0)]$; x_0 is the virtual origin and A is a constant. In the region $10 < (x+x_0)/D < 50$, Hinze & Van der Hegge Zijnen (1949) found that $A = 5{\cdot}9$ and $x_0 = -0{\cdot}5D$, and Wygnanski & Fiedler (1969) found that $A = 5{\cdot}9$ and $x_0 = -3D$. However, for a larger x-range (i.e. for $25 < (x+x_0)/D < 95$), Wygnanski & Fiedler found that $A = 5{\cdot}4$ and $x_0 = -7D$. The values of A and x_0 from the least-squares fit of our data in the region $10 \leqslant x \leqslant 45$ are given in table 2.

L_p (cm)	7·62	15·24	30·48	60·96	91·44
A	5·34	5·03	4·84	4·15	4·07
x_0/D	−3·12	−3·0	−1·29	−6·32	−6·2

TABLE 2

The discrepancies between the values of both A and x_0 obtained by various investigators may be due to different initial conditions, as also suggested by Hinze (1975). Note that values of L_p having laminar exit boundary layers have nearly the same values of A and x_0. For pipes having turbulent exit boundary layers (L_p = 60·96 and 91·44 cm) A and x_0 are nearly the same, but different from those with laminar boundary layers. The nozzle with a transitional exit boundary layer (i.e. L_p = 30·48 cm) produces a value of A intermediate between those for the laminar- and turbulent-exit cases.

The streamwise variations of $u_c'(x)/U_e$ show that the effects of the initial condition, which produces noticeable changes in the near-field $u_c'(x)$, are progressively forgotten at larger x. With an initially turbulent boundary layer, the initial growth rate of $u_c'(x)$ is slower than in the laminar case but the peak value is nearly the same. The peak value of $u_c'(x)$ seems to occur at nearly the same x ($\simeq 8D$), the location of turbulence breakdown. The decay rate of $U_c(x)$ seems to depend systematically on L_p; with increasing L_p the decay rate increases.

A stricter criterion for achievement of self-preservation of the flow is the value of u_c'/U_c, also plotted in figure 5 (see also figures 11*b* and 12*b*). The u_c'/U_c values increase with x beyond $x/D = 50$, even though the mean velocity profiles become nearly similar much earlier (discussed later). Wygnanski & Fiedler's u_c'/U_c data also increased with x but achieved a constant value of 0·28 for $x/D \gtrsim 40$. Corrsin & Uberoi's (1950) data showed u_c'/U_c increasing with x up to 0·22 (at $x/D \simeq 26$). Antonia, Satyaprakash & Hussain (1980) found the value of u_c'/U_c increasing to a value of 0·32 (at $x/D = 140$).

It is both interesting and surprising that effects of the initial condition on the mean velocity persist in the self-preserving region of the jet. In virtually all previous studies in the self-preserving region of a jet, the initial condition was never documented, presumably because of the expectation that the self-preserving flow is independent of initial condition. It is suggested that all future studies of turbulent shear flows must carefully document the initial condition. One possible explanation for the dependence of U_c in the self-preserving region on the initial condition may be that, even though the exit centre-line mean velocity U_e is the same for all the jets, the exit momentum flux is different for different L_p. For example, owing to the thicker boundary layer, the exit momentum flux for L_p = 91·44 cm is much lower than that for the L_p = 7·62 cm jet.

The self-excited jet at controlled excitation amplitudes

The jet response. The response of a jet to controlled excitation should depend on the frequency and amplitude of excitation, the exit velocity U_e, and the initial condition. Any time-average measure g of the jet can thus be written in the general functional form $g = g(R_D, M, St_D, St_\theta, \text{initial condition}, u_e'/U_e, L_c/h)$, where $St_D = fD/U_e$ and $St_\theta = f\theta/U_e$, f being the frequency of excitation. For low-subsonic jets, we may

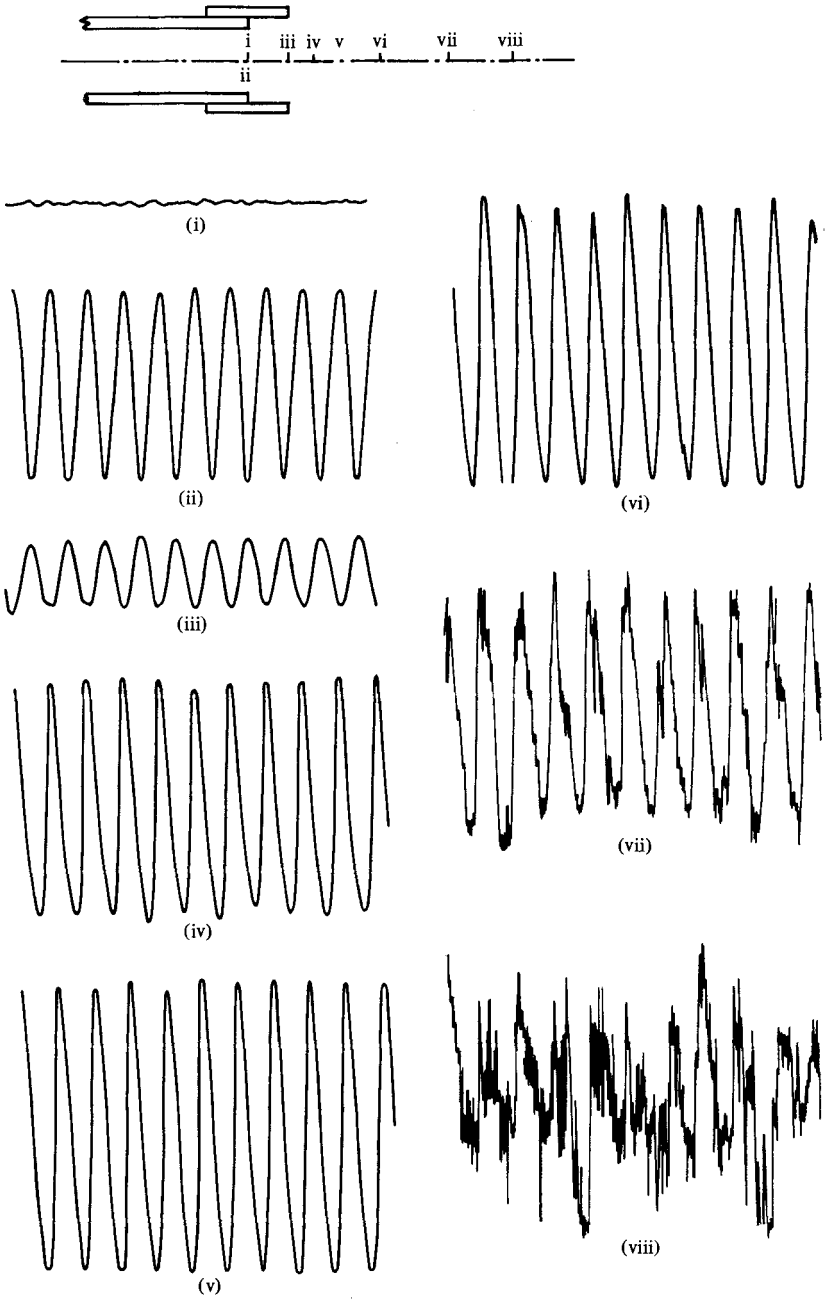

FIGURE 6. Evolution of $u(t)$ on the centre line for $L_p = 30{\cdot}48$ cm; $D = 2{\cdot}54$ cm, $U_e = 36$ m s^{-1}, $u'_e/U_e = 12\,\%$, $St_D = 0{\cdot}355$. All traces have identical horizontal and vertical scales. Trace (i) is the exit signal without excitation. x/D values for successive traces are: (ii) 0; (iii) 0·4; (iv) 1·0; (v) 1·5: (vi) 2·0; (vii) 3·0; (viii) 4·0.

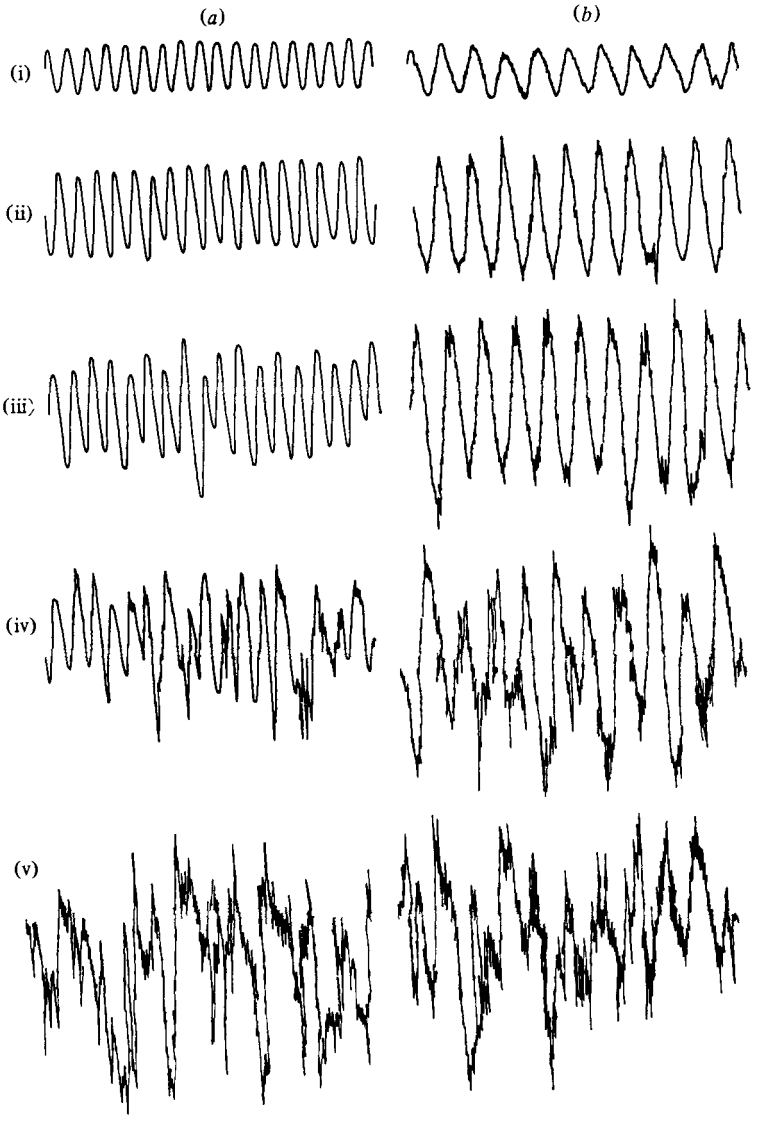

FIGURE 7. Evolution of $u(t)$ on the jet centre line for $u_e'/U_e = 3\,\%$; $U_e = 36$ m s^{-1}. (*a*) initially laminar, $L_p = 15{\cdot}24$ cm, $St_D = 0{\cdot}635$. (*b*) initially fully turbulent, $L_p = 60{\cdot}96$ cm, $St_D = 0{\cdot}38$. x/D values for the different traces are: (i) 0; (ii) 1·0; (iii) 2·0; (iv) 3·0; (v) 4·0.

disregard Mach number M as being unimportant. We believe that the primary effect of the jet speed is via the initial condition and thus the jet Reynolds number R_D; hence, though likely to be important at very low speeds, U_e is not an independent parameter provided that R_D is large enough (the effect of R_D is already included through St_D, St_θ and the initial condition). Both St_θ and St_D are irreducible parameters, the former controlling the near-exit jet behaviour and the latter controlling the jet behaviour farther downstream. As shown by Zaman & Hussain (1980), these two control the shear-layer and jet-column modes in the jet. Thus,

$$g = g(St_D, St_\theta, \text{initial condition}, u_e'/U_e,\ L_c/h).$$

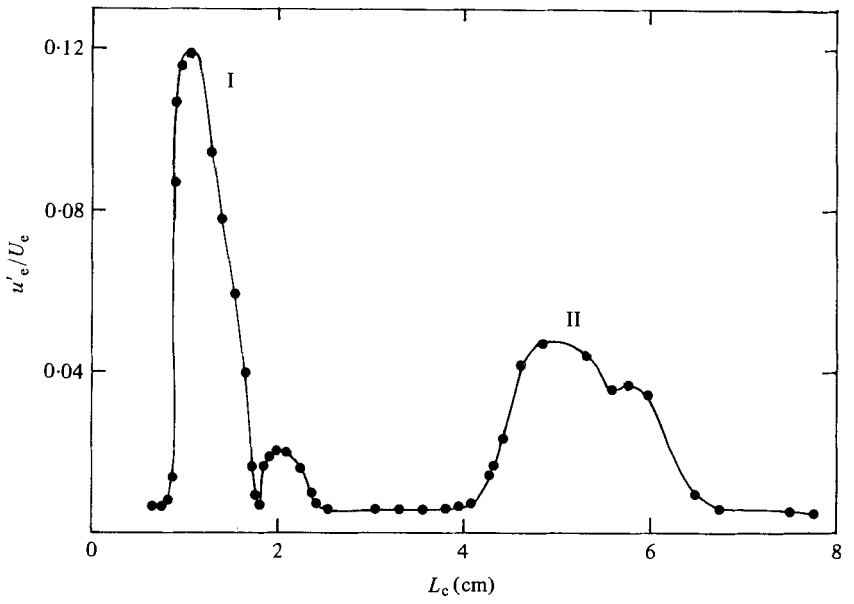

FIGURE 8. Variation of pipe-exit fluctuation intensity u'_e/U_e with collar length L_c for the L_p = 30·48 cm nozzle, U_e = 36 m s^{-1}, and D = 2·54 cm. I, II: first stage and second stage.

Streamwise evolutions of the centre-line longitudinal velocity $u_c(t)$ are shown in figure 6 for a typical case, corresponding to the maximum u'_e/U_e in the first stage of excitation. Note that the pipe exit velocity is indeed sinusoidally modulated under self-excitation and the modulation is quite strong (about 12%). The inset in figure 6 shows the relative positions of the hot wire for the different traces. At $x/D = 3$ (trace vii), turbulent fluctuations appear on the centre line, mostly during the decelerating phase of the flow. At $x/D = 4$ (trace viii), the flow is essentially turbulent but the underlying periodicity is still identifiable. Note that the frequency (f = 504 Hz; St_D = 0·355) of the periodic signal between the exit and the end of the potential core is the same. Thus, there is no vortex pairing occurring for the case recorded in figure 6. Note that the amplitude of the periodic component decreases from the exit value to a minimum at $x/D \simeq 0{\cdot}4$ (trace iii) and increases again to the maximum at $x/D \simeq 1{\cdot}5$ (trace v), before decreasing farther downstream along with progressively increasing spectral broadening.

The effects of controlled self-excitation (u'_e/U_e = 3%) on the initial evolution of the jet for the two limiting (asymptotic) initial states – laminar and fully turbulent – are captured in the $u(t)$ traces in figures 7(a,b). The frequencies of excitation in figures 7(a,b) are 900 and 540 Hz, respectively. Note that for higher and lower values of L_p (e.g. 7·62 and 91·44 cm), self-excitation cannot produce u'_e/U_e as large as 3%. The abrupt increase in amplitude in the middle of trace (iii) in figure 7(a) suggests an incipient pairing event, which was checked to be infrequent. Comparison of traces in figure 7(a) with those in figure 6 shows intermittent pairing in the former case. It is impressive that an initially fully turbulent jet can also be 'unstable' to induced self-excitation (figure (7b)). The streamwise growth of the excitation mode is larger for the initially turbulent case than for the laminar case. The presence of the induced periodicity even at $x/D = 3$ suggests that the initially fully turbulent jet is also

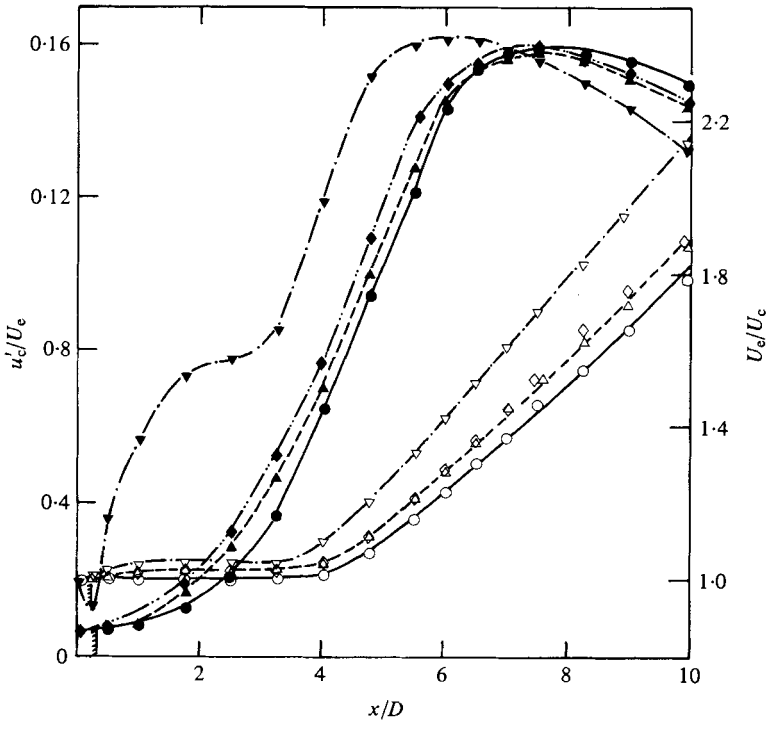

FIGURE 9. Streamwise variation of U_c (open) and u_c' (solid), showing the effect of L_c and self-excitation on U_c and u_c' for $L_p = 60{\cdot}96$ cm, $D = 7{\cdot}62$ cm, $U_e = 60$ m s^{-1}, $u_e'/U_e = 2\,\%$. The frequency of excitation (Hz) and collar length (cm) are: ○, (0, 0); △, (0, 1·65); ▽, (470, 1·78); ◇, (0, 2·41).

organized into coherent structures by the self-excitation. At $x/D = 4$, the traces (in figures 7*a*, *b*) are essentially the same; this is consistent with our observation that initial toroidal structures break down at $x/D \simeq 4$ and enhanced azimuthal coherence induced by controlled excitation cannot retard or weaken the breakdown process (Hussain & Zaman 1980).

Collar effect. Figure 8 shows the exit amplitude u_c'/U_e as a function of the collar length L_c. The distribution shown (for $h = 0{\cdot}3175$ cm) is typical of all other L_p. For the $D = 2{\cdot}54$ cm nozzle, the whistler phenomenon was investigated for values of h in the range 0·159–0·953 cm. Within this range, the excitation amplitude and the jet response (see figures 11 and 12) were not highly sensitive to h. The workable range of h, which will be determined by D, U_e and the pipe exit flow condition, was not explored. Thus, a pipe-nozzle jet can be kept in a stable state of self-sustained excitation for any exit excitation amplitude up to the maximum u_c'/U_e available (for example 12 % for figure 8). Because of the rapid rise in $u_e'(x)$ it is not possible to maintain a constant u_e'/U_e in the range 2–8 % on the left-hand side of stage I (discussed later).

The observed modifications of the jet under self-excitation ($L_c > 0$) can be the result of two independent effects: that of self-excitation and of the collar acting as a blocked-off ejector. Comparison of the self-excited-jet response to that of an externally excited jet necessitates separation of these two effects. Data presented in figure 9 isolate the effect of the collar from the effect of excitation by comparing $U_c(x)$ and

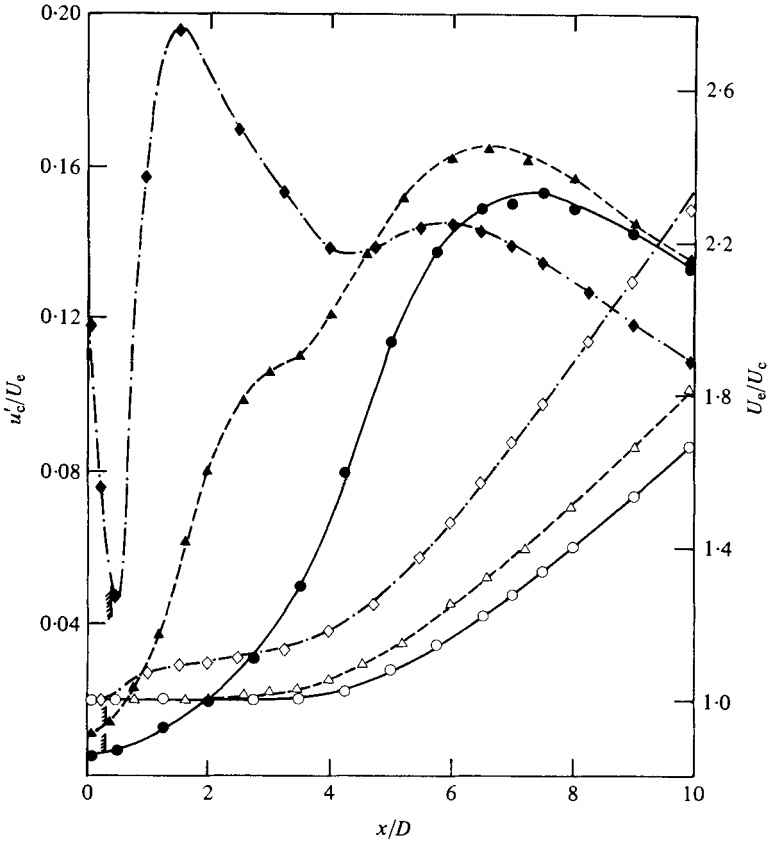

FIGURE 10. Streamwise variation of U_c (open) and u_c' (solid) showing the effect of u_e'/U_e for L_p = 30·48 cm (I), D = 2·54 cm and U_e = 36 m s^{-1}. L_c (cm), f (Hz) and u_e'/U_e' are: ○, (0·812, 0, 0·007); △, (0·83, 516, 0·011); ◇, (0·99, 504, 0·12).

$u_c'(x)$ data for four different values of L_c; note that $f = 0$ denotes no excitation. The location of the collar exit is shown by a vertical (hatched) line on the r.m.s. profiles, a notation followed in all figures. The data in figure 9 are for L_p = 60·96 cm at U_e = 60 m s^{-1} (D = 7·62 cm). Non-zero values of L_c noted (1·65 and 2·41 cm) represent the locations of the collar just before and after the first stage of excitation. The $U_c(x)$ and $u_c'(x)$ data for these two L_c and for $L_c = 0$ show that the effect of the collar itself, when the jet is unexcited, is marginal. However, for the L_c = 1·78 cm case when u_e'/U_e is 2 % (St_D = 0·594) we notice significant increase of the turbulent intensity and faster decay of the mean velocity compared with the other three cases. Considering the excited case with L_c = 1·78 cm and the unexcited case with L_c = 1·65 cm, the change in L_c is negligible. This is therefore a conclusive demonstration that modifications of the jet by the whistler nozzle are principally due to the excitation rather than being merely due to the presence of the collar.

Effect of excitation amplitude. Figure 10 shows $U_c(x)$ and $u_c'(x)$ for two different exit excitation amplitudes for the L_p = 30·48 cm nozzle. Note that a given excitation amplitude can be obtained for two different collar positions in each stage (see figure 8). The data in figure 10 correspond to the left side of the first stage in figure 8, where

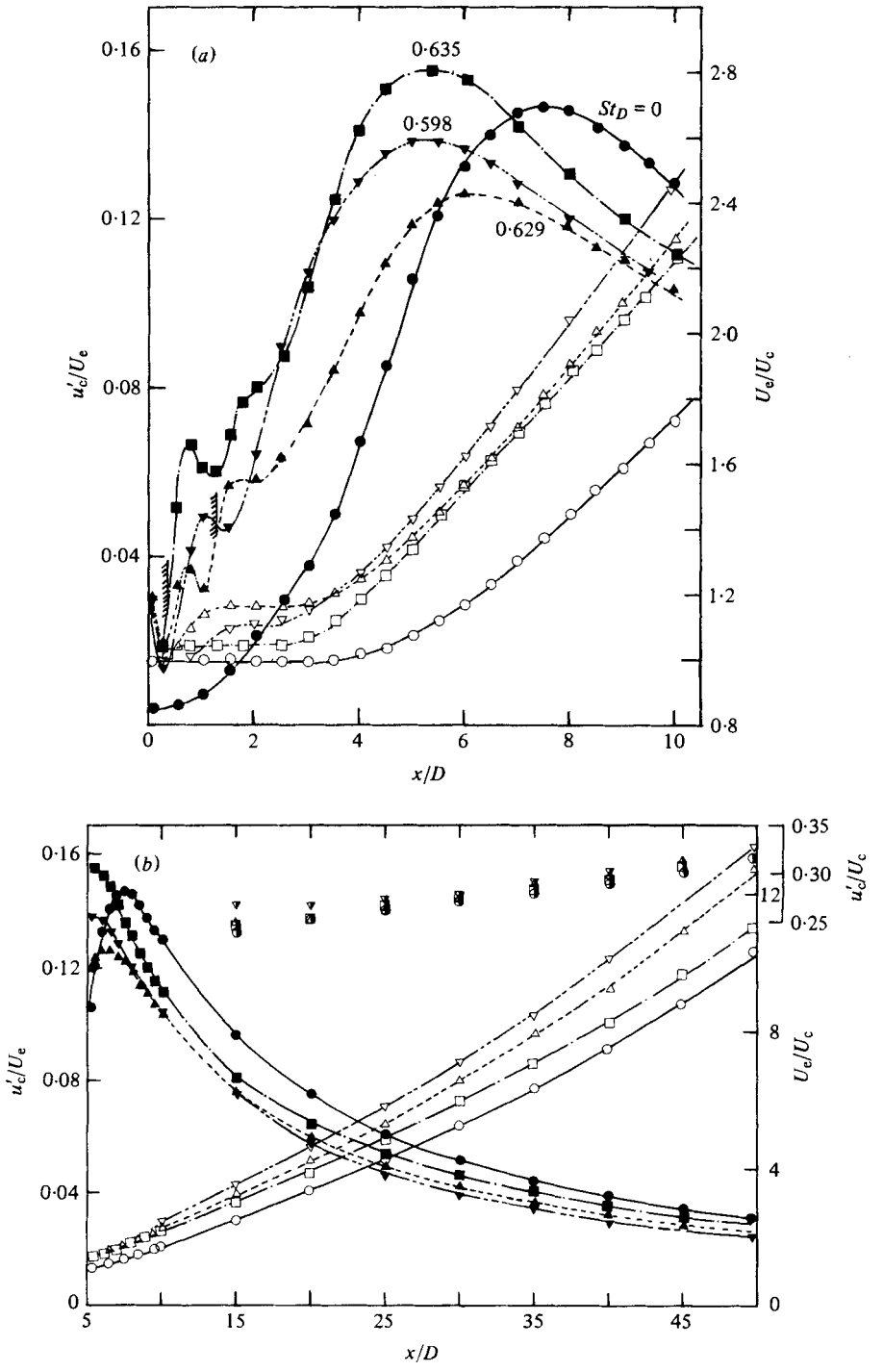

FIGURE 11. Streamwise variation of U_c (open), u_c' (solid) and u_c'/U_c (semi-open) for $L_p = 15{\cdot}24$ cm, $D = 2{\cdot}54$ cm, $U_e = 36$ m s^{-1}, $u_e'/U_e = 3\,\%$. The stage of excitation and step height (cm) are: ○, unexcited, 0·3175; □, I, 0·3175; △, II, 0·3175; ▽, II, 0·635. (*a*) Data for the range $0 \leqslant x/D \leqslant 10$. (*b*) Data for the range $5 \leqslant x/D \leqslant 50$.

u'_e/U_e rises sharply with L_c. Thus, any difference between the jet responses for the two cases would correspond to the effect of u'_e/U_e, since L_c is essentially constant. The corresponding unexcited ($L_c = 0{\cdot}812$ cm) data are also included in figure 10. Note that self-excitation produces an earlier decay of $U_c(x)$ and thus has the equivalent effect of an upstream shift of the virtual origin. When u'_e/U_e is increased from 1·1 to 12 %, $u'_c(x)/U_e$ develops a strong peak at $x/D \simeq 2$. The amplitude of the first $u'_c(x)$ peak becomes nearly independent of u'_e/U_e at values larger than 4 %, consistent with the observations of Crow & Champagne (1971) and Schmidt (1978).

The effect of the self-excitation is more dramatic on u'_c than on U_c. Note that, under excitation, $u'_c(x)$ first drops rapidly with increasing x up to $x \simeq 0{\cdot}5D$ before increasing rapidly again (when u'_e/U_e is large). At this location of minimum u'_c, the value of $u'_c(x)$ is still higher than the corresponding unexcited value. This near-exit suppression, also observed in contraction-nozzle jets by Hussain & Zaman (1975), is probably due to interference effects between hydrodynamic and acoustic waves; see also Pfizenmaier (1973) and Crighton (1972). For initially laminar jets, Zaman & Hussain (1981) have provided an explanation for the suppression effects in terms of the shear-layer instability.

In order to examine the jet response to a u'_e/U_e which is of practical interest as well as to allow comparison with earlier data with contraction nozzles (Crow & Champagne 1971; Zaman & Hussain 1980) it was decided to obtain jet data at $u'_e/U_e = 3\,\%$. In an attempt to extend the data base of the 2·54 cm nozzle, a larger jet ($D = 7{\cdot}62$ cm) was built and data were obtained with $u'_e/U_e = 2\,\%$ because a larger u'_e/U_e was not available with all L_p over the velocity range of interest.

Effects of self-excitation on $U_c(x)$ *and* $u'_c(x)$. Since the exit-flow characteristics and the self-excitation frequency depend directly on L_p, excitation data have been grouped together for each L_p. The streamwise variations of U_c and u'_c for two values of L_p are shown in figures 11 and 12. In order to highlight the effects of self-excitation, data for the first 10 diameters, where most of the changes due to self-excitation take place, are presented in expanded scales in figures 11 (*a*) and 12 (*a*). Data farther downstream are shown in figures 11 (*b*) and 12 (*b*), respectively. The stage of excitation and the corresponding St_D are noted for each curve. Note that the data for the corresponding unexcited ($St_D = 0$) case are also included in order to permit easy comparison.

The self-excitation clearly produces a large increase in the decay rate of $U_c(x)$ and almost always an upstream shift of the virtual origin. The trends of A and x_0 with L_p (not shown) are similar to those for the unexcited pipe-nozzle jets. In spite of different initial values under excitation, u'_c/U_c approaches nearly constant values at $x/D \simeq 45$ (figures 11*b*, 12*b*). The first peaks in $u'_c(x)$ for $L_p = 15{\cdot}24$ cm (at $x \simeq D$ in figure 11*a*) are due to occasional vortex pairing. This was confirmed by the subharmonic peak in $S_u(f)$ taken at the corresponding x-location on the centre line and at the transverse position where the mean velocity is $0{\cdot}95U_e$. Traces (iii) and (iv) in figure 7 (*a*) have captured such rare events of weak pairing. Note that figure 18 also shows a subharmonic for this L_p. Note that for $L_p = 30{\cdot}48$ cm, however, figures 12 (*a*) and 18 show no such peaks or subharmonic. For further discussion of those peaks see Zaman & Hussain (1980).

For the purpose of comparing effects of self-excitation with those of imposed (forced) acoustic excitation, the data of Crow & Champagne (1971) and Zaman &

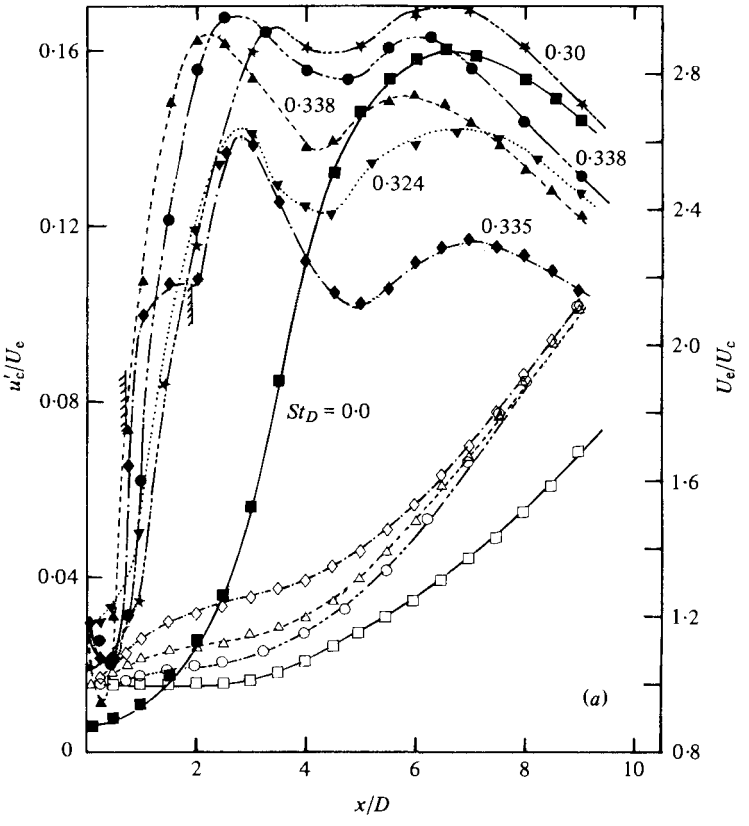

FIGURE 12 (*a*). For legend, see opposite.

Hussain (1980), rather than those of Moore (1977) or Bechert & Pfizenmaier (1975), seem appropriate because of comparable exit excitation levels and exit velocities. The $u_c'(x)$ data of Zaman & Hussain obtained by external acoustic excitation in a contraction nozzle agree qualitatively with ours (as do those of Crow & Champagne: however, for clarity, they are not shown here). Note that, while the $u_c'(x)$ data among the three self-excited cases in figure 12 (*a*) are themselves quite different, the first peak of $u_c'(x)$ in Zaman & Hussain's data are in general agreement with ours. The differences between our data and those of Zaman & Hussain are comparable to the differences between their data and those of Crow & Champagne. The differences between the present data and the data of those authors may be due partly to the collar effect discussed earlier, and partly to differences between the facilities, the initial condition and R_D.

Figure 12 (*a*) also shows the $u_c'(x)$ and $U_c(x)$ data for $L_p = 30{\cdot}48$ cm ($L_c = 0$), under artificial excitation by a loudspeaker placed in the upstream settling chamber. The responses of the pipe nozzle to self-excitation and to artificial excitations, as represented by $u_c'(x)$, show comparable trends (also at other values of L_p). When the pipenozzle jet is forced externally, U_c drops faster with x than when unforced, but this drop is never as large as for the case of self-excitation.

In figures 11 and 12, the first stage of excitation produces higher peaks in $u_c'(x)$ than the corresponding second stage. This is quite probably due to the fact that the collar

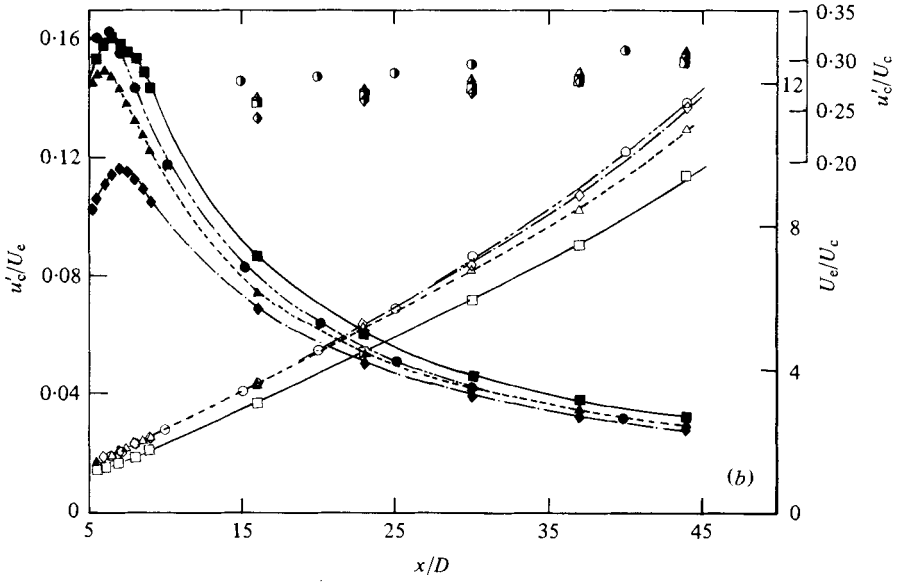

FIGURE 12. Streamwise variation of U_c (open), u_c' (solid) and u_c'/U_c (semi-open) for $L_p = 30{\cdot}40$ cm, $D = 2{\cdot}54$ cm, $U_e = 36$ m s^{-1}, $u_e'/U_e = 3$ %. The stage of excitation and step height (cm) are: □, unexcited, 0·3175; △, I, 0·3175; ○, I, 0·635; ◇, II, 0·3175. (*a*), data for the range $0 \leqslant x/D \leqslant 10$; (*b*), data for the range $5 \leqslant x/D \leqslant 50$. In (*a*): ★, Zaman & Hussain (1980) data; ▼, pipe excited by loudspeaker when $L_c = 0$.

length L_c for the first stage, being smaller than that in the second stage, induces stronger vortices whose influence, although the same at $x = 0$, is stronger farther downstream. Figures 11 and 12 also show that step height h does not have any significant effect on $u_c'(x)$ or $U_c(x)$. The amplitude of the first peak of $u_c'(x)$ in figure 11 (*a*) ($St_D \simeq 0{\cdot}64$) is lower than the peak in figure 12 (*a*) ($St_D \simeq 0{\cdot}34$); the difference is perhaps an effect associated with the value of St_D. Crow & Champagne found this peak to become a maximum at $St_D = 0{\cdot}3$, and accordingly termed it 'the preferred mode'. Zaman & Hussain (1980) demonstrated that the 'preferred mode' should be redefined and based on the fundamental amplitude only. It should be emphasized that the 'preferred mode', though identified by us with $St_D = 0{\cdot}30$, can actually occur over a range in St_D depending on R_D, initial condition, etc. (Hussain & Zaman 1981). For St_D outside the range 0·30–0·35 the amplitude of the first peak in $u_c'(x)$ is lower. Note that the differences between $u_c'(x)/U_e$ decrease with increasing x. For a turbulent exit boundary layer, self-excitation data (not shown) revealed significant differences between two values of L_p (30·48 and 60·96 cm) although the values of St_D for the two cases were identical. This would suggest that, for initially turbulent circular jets, St_D is not the only controlling parameter characterizing the turbulence structure as suggested by Crow & Champagne's results. The large differences in the near-field $u_c'(x)$ data at the same St_D are perhaps due to differences in R_D, initial condition, etc. (see also Hussain 1981).

Figure 13 shows $U_c(x)$ and $u_c'(x)$ for the $D = 7{\cdot}62$ cm jet at 60 m s^{-1}. Like the 2·54 cm diameter jet data, self-excitation increases the mean velocity decay rate and

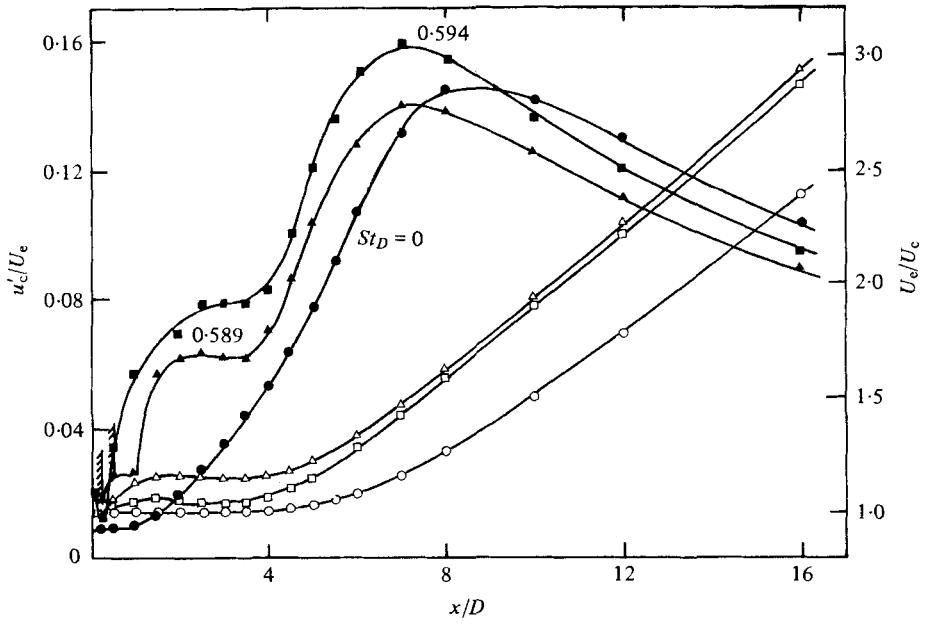

FIGURE 13. Streamwise variation of U_c (open) and u_c' (solid) for L_p = 60·96 cm, D = 7·62 cm, H = 0·635 cm, U_e = 60 m s^{-1}, u_e'/U_e = 2 %. ○, unexcited; □, stage I; △, stage II.

enhances the near-field fluctuation intensity. Note that the two stages, at essentially the same St_D, produce more variations in $u_c'(x)$ than in $U_c(x)$. These data show effects of excitation on an incompressible circular jet at perhaps the highest Reynolds number ($3{\cdot}06 \times 10^5$) reported so far.

Although Bechert & Pfizenmaier (1975), Moore (1977) and Schmidt (1978) have introduced a pure-tone acoustic excitation in a circular jet, the excitation levels and velocities used by them were too different from ours to allow any meaningful comparison with our data. In addition, our experiment did not involve any acoustic measurement.

A question arises as to the role of the initial condition in the modification of jet behaviour by self-excitation. For the unexcited jet (figure 5), we have seen that $U_c(x)$ and $u_c'(x)$ vary systematically with L_p (for $L_c = 0$) thus confirming the dependence of the jet characteristics on the initial condition. However, this dependence on L_p is not as strong as that of an excited jet (figures 11*a*, 12*a*). Since figures 11(*a*) and 12(*a*) have two different values of St_D, it is necessary to demonstrate the effect of initial condition on self-excitation for the same St_D. This was done in two different ways: first, by tripping the L_p = 15·24 cm nozzle so that the St_D of excitation was the same for untripped (figure 11(*a*)) and tripped (not shown) pipe-nozzle jets of the same L_p; and secondly, by comparing the half-wave-mode excitation data of the L_p = 30·48 cm (figure 12(*a*)) nozzle with the full-wave-mode excitation data of the L_p = 60·96 cm nozzle (not shown). These two sets of data (each at the same St_D) showed that the $U_c(x)$ and $u_c'(x)$ distributions were significantly dependent on the initial condition. It should also be emphasized that the relative change brought about by self-excitation is about the same for a given initial condition (say, laminar or turbulent).

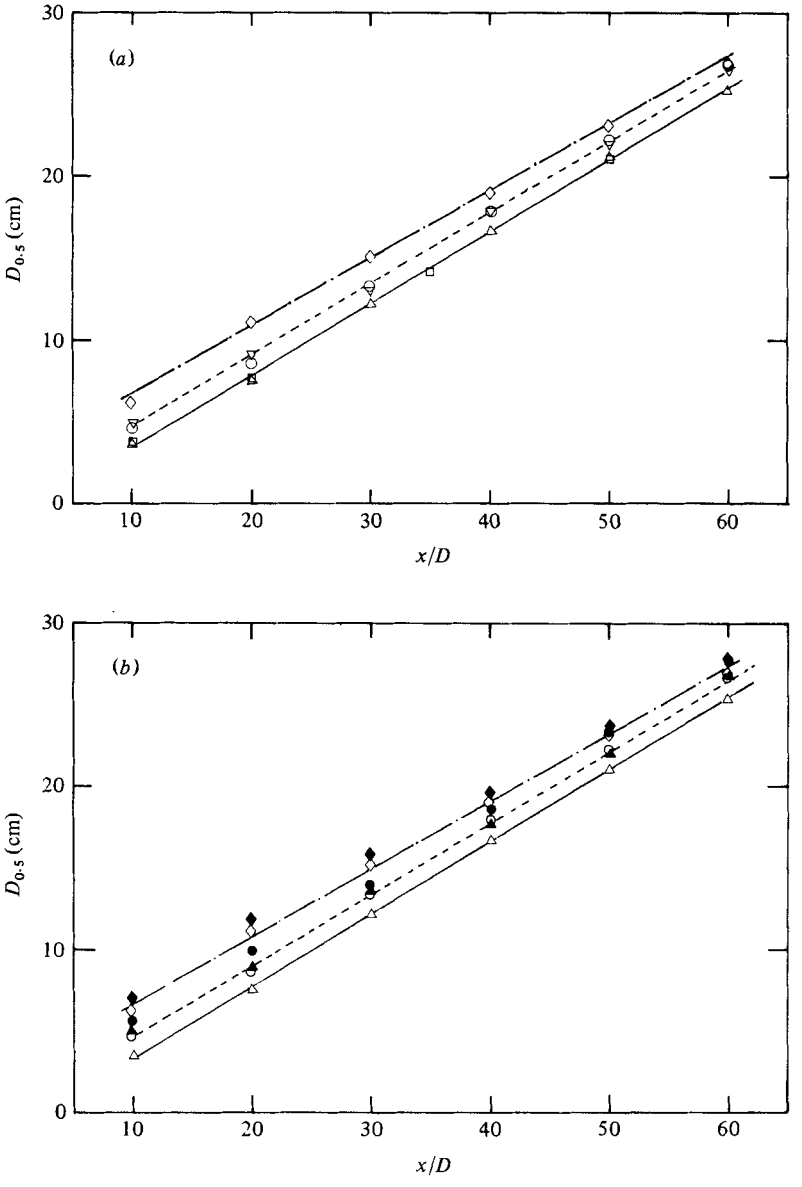

FIGURE 14. (*a*) Axial variation of jet half-width $D_{0.5}$ for different nozzles without excitation for $D = 2{\cdot}54$ cm and $U_e = 36$ m s^{-1}. The nozzle lengths L_p are: ▽, 7·62; ○, 15·24; ◇, 30·48; △, 60·96; □, 91·44. (*b*) Axial variation of half-width $D_{0.5}$ for unexcited (open symbols) and first-stage excitation (solid symbols) with $u'_e/U_e = 3\,\%$. Symbols as in (*a*).

The jet width and spread rate. The diameter $D_{0.5}$ corresponding to the locations of the half-mean maximum velocity, i.e. $0{\cdot}5U_c$, in the profile at each x has been measured. Figure 14(*a*) shows the jet width $D_{0.5}$ for the unexcited jets with different L_p. The jet width for each case increases linearly with x. It is clear that both the jet width $D_{0.5}$ and the spread rate $dD_{0.5}/dx$ depend on L_p, i.e. on the initial condition. Jets from pipe nozzles with initially turbulent exit flows produce minimum spreads. Since initially turbulent shear layers spread faster (Hussain & Zedan 1978), the initial region should

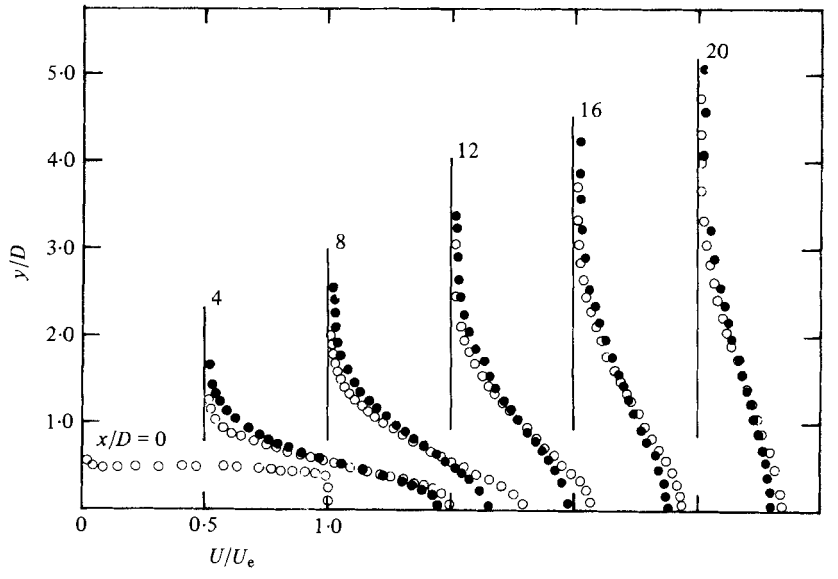

FIGURE 15. Evolution of mean-velocity profiles for unexcited (open symbols) and excited (solid symbols) (first-stage) cases for $L_p = 60{\cdot}96$ cm, $D = 7{\cdot}62$ cm, $U_e = 60$ m s^{-1}.

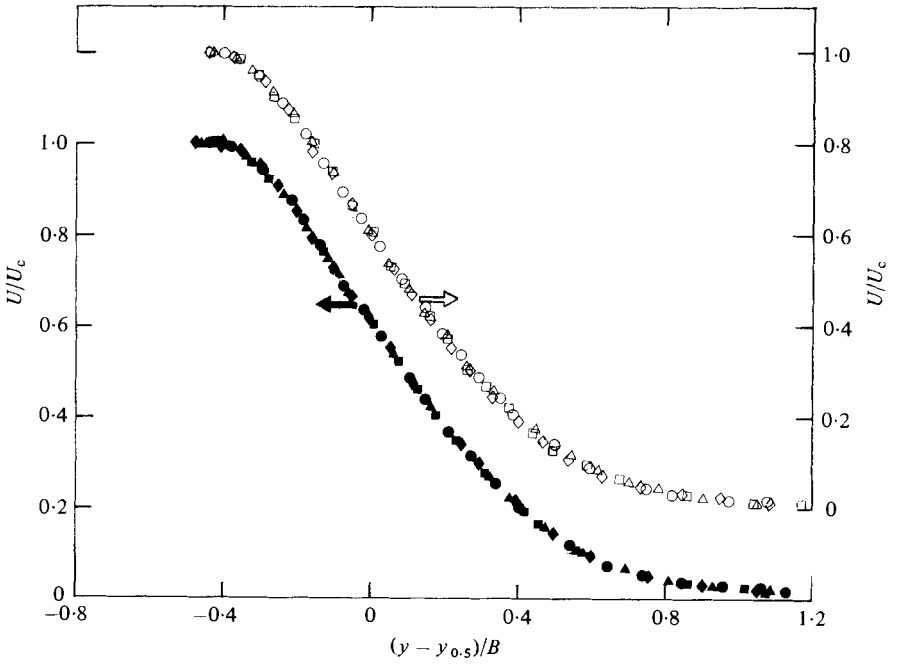

FIGURE 16. Mean-velocity profiles of figure 15 showing similarity. x/D values are: ○, 8·0; □, 12·0; △, 16·0; ◇, 20·0.

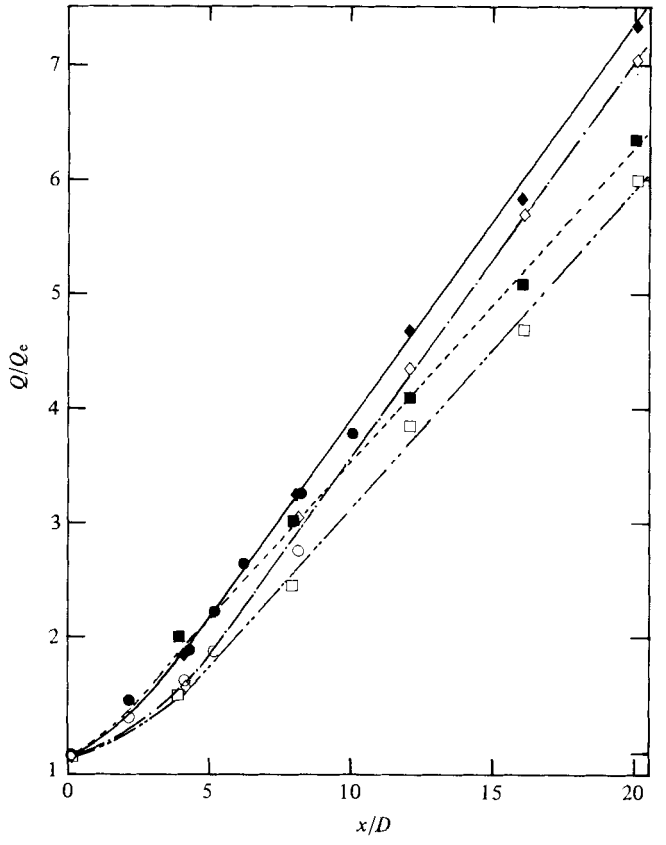

FIGURE 17. Streamwise evolutions of the volume flux Q/Q_e for unexcited (open symbols) and excited (solid symbols) cases: ◇, D = 2·54 cm; □, D = 7·62 cm; ○, Crow & Champagne (1971).

be shorter for turbulent-exit cases. In spite of this, the lower spreads of the jets suggest smaller-sized coherent structures for initially turbulent cases (Clark 1979). The L_p = 30·48 cm pipe nozzle, which has a transitional initial boundary layer, produces maximum spread. Note that the jet spreads fall into three classes, indicated by the three straight lines in figure 14(*a*), the spread for the initially turbulent cases being the lowest and that for the initially transitional case being highest.

Comparing the $D_{0.5}(x)$ data with the corresponding $U_c(x)$ data in figure 5, it is clear, as was suspected, that the streamwise variations $D_{0.5}(x)$ and $U_c(x)$ do not correspond directly with each other. While the decay in $U_c(x)$ with increasing x clearly depends on L_p, the spread variations $D_{0.5}(x)$ as well as the spread rate $dD_{0.5}/dx$ show no such trends. Kotsovinos (1976) pointed out that the spread of a plane jet does not increase linearly with x but weakly nonlinearly. Bradshaw (1977) speculated that this non-linear variation is produced by recirculation and turbulence in the laboratory, and that spread in a circular jet should be similarly nonlinear. Bradshaw could not verify his speculation for the circular jet because of non-availability of circular-jet data in the literature. Our data indicate that, within the uncertainty of the data, $D_{0.5}(x)$ is linear for each of the five initial conditions studied. The linear increase of $D_{0.5}(x)$ with

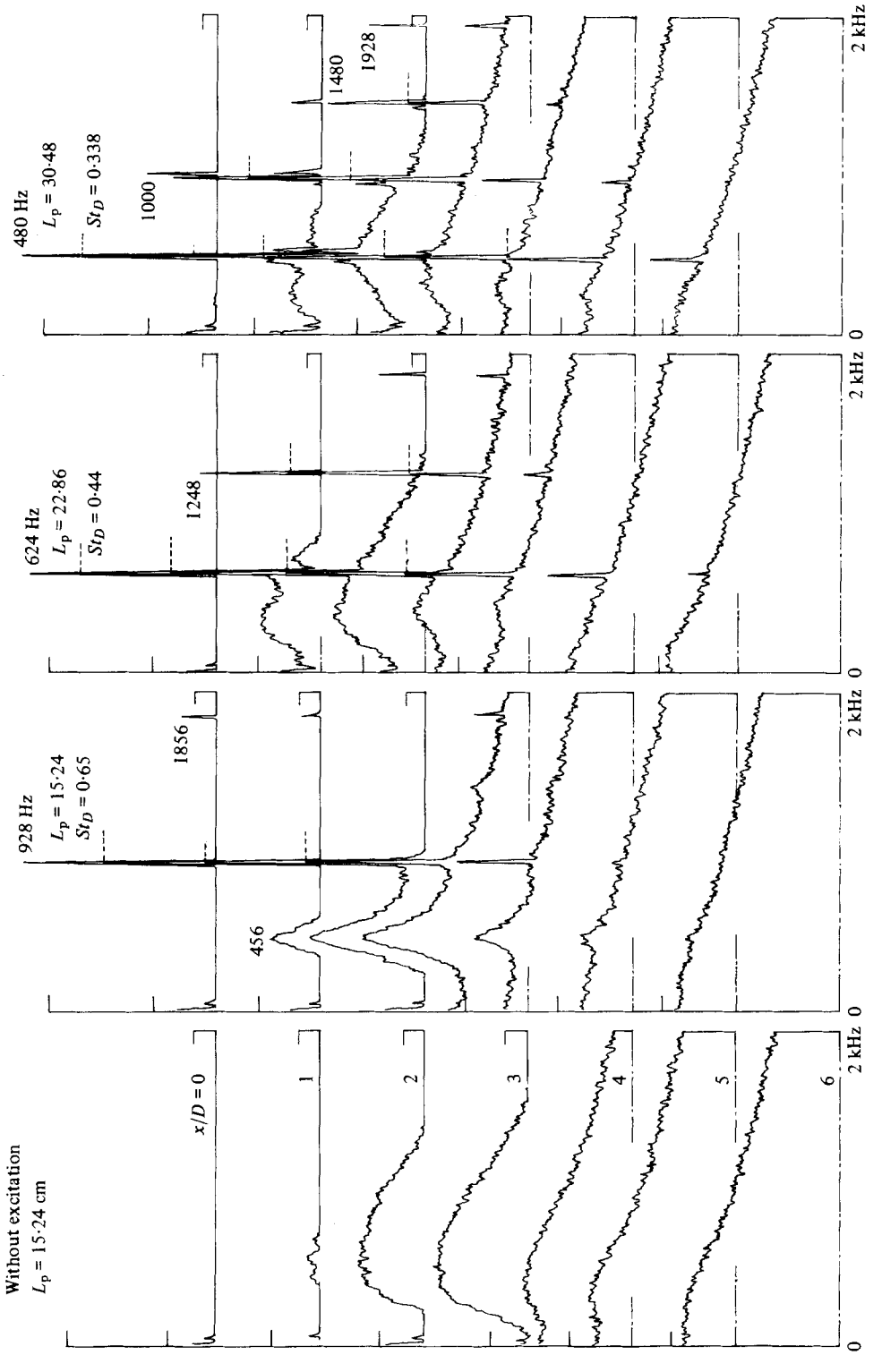

FIGURE 18. Evolution of the u-spectrum on the jet centre-line for L_p = 15·24, 22·86 and 30·48 cm, for D = 2·54 cm at U_e = 36 m s^{-1}; u_e'/U_e = 3 %.

x while $U_c(x)$ drops slightly faster than x^{-1} is a contradiction if constant momentum flux in the self-preserving region is assumed. The nonlinear variation of U_c^{-1} with x, an observation common to all reported jet data, was discussed earlier.

Figure 14(*b*) compares the jet spread $D_{0.5}(x)$ for the first stage of excitation, for different L_p, with the corresponding unexcited data; the three straight lines are copied from figure 14(*a*). Note that self-excitation increases the spread of the jet in all three cases. The spread under self-excitation remains linear; the spread rate $dD_{0.5}/dx$ is essentially constant and remains unchanged between the excited and unexcited cases.

Effect of excitation on mass flux and entrainment. In order to examine the effects of self-excitation on the mass flux and entrainment in the jet, radial profiles of the mean velocity $U(y)$ have been measured at a number of x-stations. Evolutions of the $U(y)$ profiles for one representative case, $D = 7{\cdot}62$ cm, are shown in figure 15. This figure represents the excitation case in the first stage and the corresponding unexcited case. Note that for the excitation case the exit profiles are not shown, since the hot wire at $x = 1$ mm downstream from the pipe nozzle cannot detect the location of the wall in the presence of backflow when $L_c > 0$. The effect of self-excitation is clear in this figure: excitation increases the spread and the centre-line mean-velocity decay rate.

In order to examine the similarity of these profiles, these data are plotted in figure 16 as a function of $(y-y_{0.5})/B$, where the thickness of the shear region is defined as $B = y_{0.95} - y_{0.1}$. The radial locations $y_{0.95}$, $y_{0.5}$ and $y_{0.1}$ correspond to the radii where the values of U/U_c are 0·95, 0·50 and 0·1, respectively. It is clear that the velocity profiles achieve essential similarity in the jet for both the unexcited and excited cases. Similar collapse of the data is obtained when y is non-dimensionalized by the local profile momentum thickness θ, defined as

$$\theta \equiv \int_{y_{0.1}}^{0.95} (U/U_c)(1 - U/U_c)\, dy.$$

Volume fluxes were computed from the profiles shown in figure 15 by performing the integration

$$Q(x) = \int_0^{y_{0.01}} 2\pi y U(y)\, dy.$$

The data at large radii, i.e. at locations of low U/U_c, were smoothed by fitting them with a profile of the form $U/U_c = e^{-c(y/x)^2}$. This analytical expression was then used for generating data at the outer radii where the hot-wire measurements are inaccurate owing to the effects of large fluctuation intensity and even flow reversal (Chevray & Tutu 1978; Hussain & Zaman 1980). Note that the integration was terminated at $y_{0.01}$, corresponding to $U/U_c = 0{\cdot}01$, because U/U_c becomes zero only at infinite radius. Data for the 2·54 cm jet showed comparable effects of excitation on $U(y)$ and comparable collapse of U as a function of $(y-y_{0.5})/B$. These non-dimensional data look essentially identical with those in figures 15, 16 and are not shown.

Figure 17 shows the streamwise variations of the volume flux Q/Q_e for both $D = 2{\cdot}54$ cm and $D = 7{\cdot}62$ cm cases; Q_e is the exit volume flux. The data of Crow & Champagne (1971) are also included for comparison. For both jet sizes, the volume flux increases linearly with x beyond $x/D \simeq 4$. The curves for the excited and unexcited cases have equal slopes, indicating that self-excitation produces only an

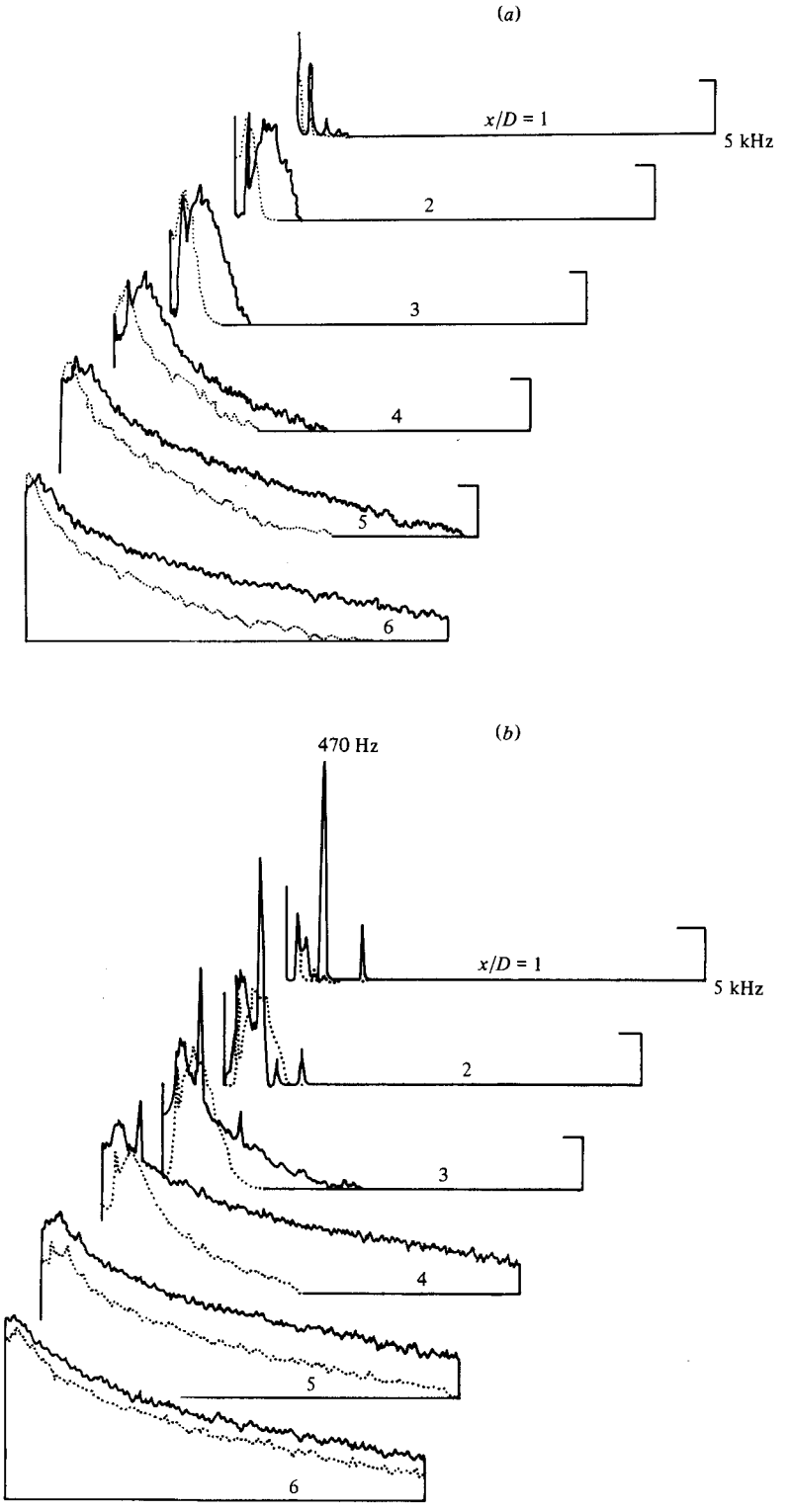

FIGURE 19 (*a*, *b*). For legend, see opposite.

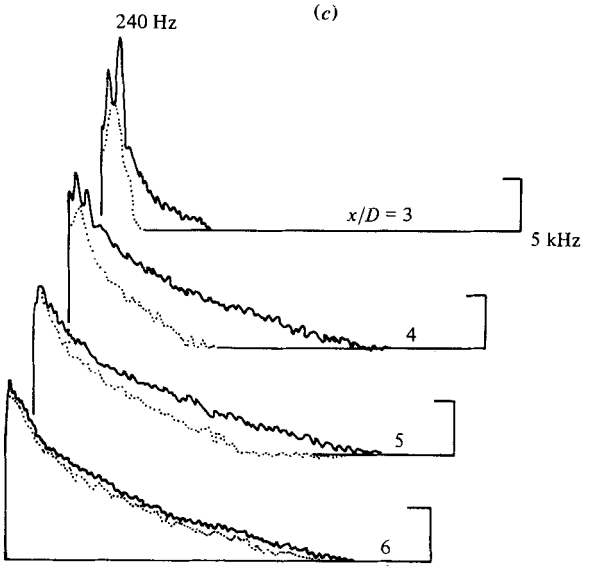

FIGURE 19. (*a*) Evolution of the unexcited u-spectrum on the jet centre line for $L_p = 60{\cdot}96$ cm, $D = 7{\cdot}62$ cm. Solid, $R_D = 3{\cdot}1 \times 10^5$; dotted, $R_D = 1{\cdot}55 \times 10^5$. (*b*, *c*) Evolution of u-spectrum on the jet centre line for $L_p = 60{\cdot}96$ cm, $D = 7{\cdot}62$ cm at $St_D = 0{\cdot}6$. Solid, $u'_e/U_e = 2\,\%$; dotted, unexcited. (*b*) $R_D = 3{\cdot}06 \times 10^5$; (*c*) $R_D = 1{\cdot}53 \times 10^5$.

upstream shift of the virtual origin, without producing a noticeable change in the entrainment rate. The values of the non-dimensional entrainment rate

$$E = d(Q/Q_e)/d(x/D)$$

are 0·29 and 0·34 for the two jets over the streamwise ranges $4 < x/D < 20$. The difference in E is probably due partly to the different Reynolds numbers in the two cases, i.e. $6{\cdot}2 \times 10^4$ and $3{\cdot}06 \times 10^5$. Wygnanski & Fiedler (1969) obtained a value of 0·456 for E, which was much higher than the values obtained by us or by Crow & Champagne. The latter authors attributed this discrepancy to the assumed functional form of $U(y)$ being inappropriate for calculating volume flux in a circular jet. Their recalculation of the asymptotic jet profile measured by Wygnanski & Fiedler produced a value of $E = 0{\cdot}263$ for Wygnanski & Fiedler's jet. Note that the values of E measured by Ricou & Spalding (1961) and Hill (1972) by the completely independent 'porous-wall technique' were both 0·32, which is within the range of our results.

Spectral evolution under self-excitation. The evolution of the longitudinal velocity spectrum $S_u(f)$ under self-excitation at $u'_e/U_e = 3\,\%$ is shown in figure 18 for three different values of L_p at $R_D = 6{\cdot}2 \times 10^4$. The spectrum for the unexcited jet (for $L_p = 15{\cdot}24$ cm) is also shown. The values of St_D for the three cases are 0·338, 0·44 and 0·65, respectively. Note that the peak of the fundamental for the lowest St_D survives farthest downstream. Similar St_D dependence was also observed by Chan (1974) in the external acoustic excitation study of a contraction-nozzle jet. The strong subharmonic observed at $St_D = 0{\cdot}65$ ($L_p = 15{\cdot}24$ cm) compares well with that observed by Crow & Champagne (1971) in the forced acoustic excitation of contraction-nozzle jets. However, Zaman & Hussain (1980) found this to occur at $St_D \simeq 0{\cdot}85$, the condition for stable vortex pairing. Since Crow & Champagne limited their study to the

St_D range 0·15–0·60, it is quite likely that they would have found the strongest subharmonic to occur at a value of St_D somewhat higher than 0·6.

A survey of the recent experiments regarding the acoustic field of subsonic axisymmetric jets subjected to controlled forced excitation reveals two different types of jet response at $St_D \simeq 0{\cdot}5$, depending on the value of R_D (Crighton 1981). For $R_D < 10^5$, jets with initially laminar shear layers show an amplification for excitation at $St_D \simeq 0{\cdot}5$ and a suppression of broad-band levels. On the other hand, when $R_D \gtrsim 10^5$ and the initial shear layer is turbulent, excitation at $St_D \simeq 0{\cdot}5$ produces broad-band amplification. The second type of response is much more likely to be relevant to practical jet engines.

Figure 19(*a*) depicts the spectral evolution along the centre line of the unexcited jet for $D = 7{\cdot}62$ cm at two values of R_D ($1{\cdot}53 \times 10^5$ and $3{\cdot}06 \times 10^5$). Note that the bandwidth as well as the level of the spectrum is higher at the larger R_D. That is, spectral broadening is faster at higher R_D. Since both jets are initially turbulent, this is not an effect of the initial condition.

The effect of excitation ($u'_e/U_e = 2\,\%$) at $R_D = 3{\cdot}06 \times 10^5$ and $St_D = 0{\cdot}595$ is shown in figure 19(*b*). The corresponding unexcited spectra are shown by dotted lines. Note the large increase of the broad-band turbulence level for $x/D \gtrsim 3$. Even though a similar increase occurs at $R_D = 1{\cdot}53 \times 10^5$ and $St_D = 0{\cdot}601$ (figure 19(*c*)), note that the increase is larger for the larger R_D. Since most of the jet noise originates from the region $3 \lesssim x/D \lesssim 6$, it is thus not surprising that controlled excitation of a large-R_D jet produces broad-band noise amplification (Bechert & Pfizenmaier 1975; Moore 1977), presumably via breakdown of large-scale coherent structures into three-dimensional substructures (Hussain & Zaman 1980). Consideration of figures 19(*b*, *c*) shows that the maximum broad-band increase for both values of R_D occurs at $x/D \simeq 4$, which is likely to be the location of peak noise production at the same St_D (see also Juvé, Sunyach & Comte-Bellot 1980). It also appears that the relative amplification at the higher R_D, as compared to the lower R_D, is also the largest at this location.

The signal from a hot wire, when it is located at the end ($x/D \simeq 4$) of the jet potential core, is sufficient to characterize the overall turbulence activity at that station. Even if it is moved upstream within the potential core, it will sense the 'footprint' of the structures and their interactions in the axisymmetric mixing layer. The footprint is stronger for the larger as well as the more energetic structures. Therefore a hot wire, located on the centre line at the end of the potential core of an incompressible jet, does indeed capture the 'spectral signature' of the noise-producing events, which are presumed to be both energetic and large-scale.

Differences between the values of a characteristic measure of a jet can occur as a result of different initial and boundary conditions, Strouhal numbers and Reynolds numbers. We have shown that the effects of excitation are not due directly to the presence of the collar. The pipe-exit boundary layers in both these cases are fully developed and identical in all measurable details. So, the initial conditions for the data in figures 19(*b*, *c*) were the same. The values of L_p, the flow geometry and the environment were identical for both data sets. The Strouhal numbers for both cases were also the same. Hence, the differences between the broad-band amplifications shown in figures 19(*b*, *c*) are attributable only to the Reynolds numbers.

4. Concluding remarks

Spurred on by the possibility that the self-excitation of a pipe-nozzle jet may be useful in a number of applications, the characteristics of self-excited circular air jets have been explored. In order to characterize clearly the jet response, its behaviour has been studied at fixed values of R_D and the excitation amplitude. Self-excitation produces a faster decay of the time-mean velocity, larger fluctuation intensity in the near field, and a higher spread and entrainment. The spread was found to be linear up to $x/D \simeq 60$, and the spread and entrainment rates for $x/D \gtrsim 10$ are found to be unaffected by the self-excitation. The effects of self-excitation are qualitatively similar to those in both pipe-nozzle and contraction-nozzle jets forced acoustically by loudspeakers at corresponding St_D and R_D (up to $x/D \gtrsim 6$), even though there are noticeable differences as revealed by $U_c(x)$, $u_c'(x)$ and $S_u(f, x)$. The changes in $U_c(x)$ and $u_c'(x)$ introduced by self-excitation are primarily the effects of excitation and are not due to the concomitant interference of the collar itself. The effects of self-excitation are dependent on the initial condition much more strongly than those corresponding to the unexcited jets. The effects of the stage of excitation are essentially independent of the initial condition and the mode (half-wave or full-wave) of excitation. The first stage of excitation always produces the largest increase of the near-field fluctuation intensity. Spectral broadening, which occurs faster at higher R_D, is hastened by controlled excitation, which also introduces broad-band turbulence amplification. This amplification is the highest at the largest R_D, thus providing some support for Crighton's (1981) speculation about the R_D effect. Note that the broad-band amplification is largest at $x/D \simeq 4$, which is also the location of peak noise production. Hussain & Zaman's (1981) results, showing that with increasing R_D (up to $1{\cdot}1 \times 10^5$), the 'preferred-mode' large-scale coherent structures are more compact and produce a comparatively larger share of the coherent Reynolds stress, are also consistent with this speculation. Spectral evolution and large-scale coherent structures (excited and unexcited) are being studied in a larger incompressible-flow jet (at $R_D \simeq 8 \times 10^5$) in our laboratory.

Self-excited axisymmetric jets with pipe nozzles clearly have exciting possibilities, especially for controlling or modifying near-field transport phenomena including mixing of heat, mass, and momentum, entrainment, and aerodynamic noise generation. Some experiments in this direction are planned for the future. In this paper, only the time-mean characteristics have been captured. It was considered important to first define the limits of the parameters under which the phenomenon occurs, and document simple time-mean measures which are of technological importance. The variety of conditions for the occurrence of the phenomenon and the associated coherent structures that will have to be considered make studies of the coherent structure details prohibitive (Hussain & Zaman 1980). One, or at best two, cases should be carefully chosen for detailed study of the coherent structures. The data in this paper now provide bases for a judicious choice of one or two such specific conditions for detailed study of the large-scale coherent-structure dynamics in a self-excited jet, should one find enough justification for doing so.

This paper documents the jet response to the self-excitation. The phenomenon at work will be described and documented in a subsequent paper.

We are grateful to Drs D. Bechert and G. H. Koopmann for illuminating discussions on the data and careful reviews of the manuscript. This research, which was mostly a part of the M.S. thesis of M. A. Z. Hasan, was funded by the N.A.S.A. Langley Research Center under Grant NSG-1475 and the National Science Foundation under Grant ENG-7822110.

REFERENCES

ACTON, E. 1980 *J. Fluid Mech.* **98**, 1.

ANTONIA, R. A., SATYAPRAKASH, B. R. & HUSSAIN, A. K. M. F. 1980 *Phys. Fluids* **23**, 695.

BATT, R. G. 1978 *J. Fluid Mech.* **82**, 53.

BECHERT, D. & PFIZENMAIER, E. 1975 *J. Sound Vib.* **43**, 581.

BRADSHAW, P. 1977 *J. Fluid Mech.* **80**, 795.

BROWAND, F. K. & LAUFER, J. 1975 *Turb. Liquids* **5**, 333.

BROWN, G. L. & ROSHKO, A. 1974 *J. Fluid Mech.* **64**, 775.

BRUUN, H. H. 1977 *J. Fluid Mech.* **64**, 775.

CANTWELL, B., COLES, D. & DIMOTAKIS, P. E. 1978 *J. Fluid Mech.* **87**, 641.

CHANDRSUDA, C., MEHTA, R. D., WEIR, A. D. & BRADSHAW, P. 1978 *J. Fluid Mech.* **85**, 693.

CHAN, Y. Y. 1974 *Phys. Fluids* **17**, 46.

CHEVRAY, R. & TUTU, N. K. 1978 *J. Fluid Mech.* **88**, 133.

CLARK, A. R. 1979 Ph.D. dissertation, University of Houston.

COLES, D. 1962 *Rand Corporation Rep.* no. R-403-PR.

CORRSIN, S. & UBEROI, M. S. 1950 *N.A.C.A. Rep.* 988.

CRIGHTON, D. G. 1972 *J. Fluid Mech.* **77**, 397.

CRIGHTON, D. G. 1981 Lecture Notes in Physics (ed. J. Jimenez), vol. 136, p. 340. Springer.

CROW, S. C. & CHAMPAGNE, F. H. 1971 *J. Fluid Mech.* **48**, 547.

DAVIES, P. O. A. L. & YULE, A. J. 1975 *J. Fluid Mech.* **69**, 513.

FFOWCS WILLIAMS, J. E. & KEMPTON, A. J. 1978 *J. Fluid Mech.* **84**, 673.

FREYMUTH, P. 1966 *J. Fluid Mech.* **25**, 683.

HASAN, M. A. Z. 1978 M.S. thesis, University of Houston.

HASAN, M. A. Z. & HUSSAIN, A. K. M. F. 1979 *J. Acoust. Soc. Am.* **65**, 1140.

HILL, B. J. 1972 *J. Fluid Mech.* **51**, 773.

HILL, W. G. & GREENE, P. R. 1977 *Trans. A.S.M.E.* I, *J. Fluids Engng* **99**, 520.

HINZE, J. O. 1975 *Turbulence*, 2nd edn. McGraw-Hill.

HINZE, J. O. & VAN DER HEGGE ZIJNEN, B. G. 1949 *Appl. Sci. Res.* **1A**, 435.

HUSAIN, Z. D. & HUSSAIN, A. K. M. F. 1979 *A.I.A.A. J.* **12**, 48.

HUSSAIN, A. K. M. F. 1981 Lecture Notes in Physics (ed. J. Jimenez), vol. 136, p. 252. Springer.

HUSSAIN, A. K. M. F. & REYNOLDS, W. C. 1970 *J. Fluid Mech.* **41**, 241.

HUSSAIN, A. K. M. F. & THOMPSON, C. A. 1980 *J. Fluid Mech.* **100**, 397.

HUSSAIN, A. K. M. F. & ZAMAN, K. B. M. Q. 1975 In *Proc. 3rd Interagency Symp. Transp. Noise, University of Utah*, p. 314.

HUSSAIN, A. K. M. F. & ZAMAN, K. B. M. Q. 1980 *J. Fluid Mech.* **101**, 493.

HUSSAIN, A. K. M. F. & ZAMAN, K. B. M. Q. 1981 *J. Fluid Mech.* **110**, 39.

HUSSAIN, A. K. M. F. & ZEDAN, M. F. 1978 *Phys. Fluids* **21**, 1100.

JUVÉ, D., SUNYACH, M. & COMTE-BELLOT, G. 1980 *J. Sound Vib.* **71**, 319.

KHALIFA, M. A. & HUSSAIN, A. K. M. F. 1979 *Bull. Am. Phys. Soc.* **24**, 1128.

KIBENS, V. 1980 *A.I.A.A. J.* **18**, 434.

KOTSOVINOS, N. E. 1976 *J. Fluid Mech.* **77**, 305.

MIKSAD, R. W. 1972 *J. Fluid Mech.* **56**, 695.

MOORE, C. J. 1977 *J. Fluid Mech.* **80**, 321.

PERRY, A. E. & MORRISON, G. L. 1971 *J. Fluid Mech.* **47**, 765.
PETERSEN, R. A., KAPLAN, R. E. & LAUFER, J. 1974 *N.A.S.A.* CR-134733.
PFIZENMAIER, E. 1973 Doktor-Ingenieur-Thesis, Technische Universität Berlin.
PUI, N. K. & GARTSHORE, I. S. 1979 *J. Fluid Mech.* **91**, 111.
RICOU, F. P. & SPALDING, D. B. 1961 *J. Fluid Mech.* **11**, 21.
SCHMIDT, C. 1978 *J. Sound Vib.* **61**, 148.
SCHUBAUER, G. B. & SKRAMSTAD, H. K. 1947 *J. Aero. Sci.* **14**, 69.
SOKOLOV, M., HUSSAIN, A. K. M. F., KLEIS, S. J. & HUSAIN, Z. D. 1980 *J. Fluid Mech.* **98**, 97.
TENNEKES, H. & LUMLEY, J. L. 1974 *A First Course in Turbulence.* MIT Press.
TSO, J., KOVASZNAY, L. S. G. & HUSSAIN, A. K. M. F. 1980 *A.I.A.A.* Paper no. 80-1355.
WINANT, C. D. & BROWAND, F. K. 1974 *J. Fluid Mech.* **63**, 237.
WYGNANSKI, I. & FIEDLER, H. 1969 *J. Fluid Mech.* **38**, 577.
YULE, A. J. 1978 *J. Fluid Mech.* **89**, 413.
ZAMAN, K. B. M. Q. 1978 Ph.D. dissertation, University of Houston.
ZAMAN, K. B. M. Q. & HUSSAIN, A. K. M. F. 1980 *J. Fluid Mech.* **101**, 449.
ZAMAN, K. B. M. Q. & HUSSAIN, A. K. M. F. 1981 *J. Fluid Mech.* **103**, 133.
ZILBERMAN, M., WYGNANSKI, I. & KAPLAN, R. E. 1977 *Phys. Fluids Suppl.* **20**, S258.